CANCER DIAGNOSIS VIA ELASTIC SCATTERING SPECTROSCOPY

by

Filiz Ateş

B.Sc. in Electronic Engineering, Istanbul University, 2003

Submitted to the Institute of Biomedical Engineering
in partial fulfillment of the requirements
for the degree of
Master of Science
in
Biomedical Engineering

Boğaziçi University
2005

CANCER DIAGNOSIS VIA ELASTIC SCATTERING SPECTROSCOPY

APPROVED BY:

Assist.Prof. Murat Gülsoy .....
(Thesis Supervisor)

Assist. Prof. Ata Akın .....

Assist.Prof. Can A. Yücesoy .....

DATE OF APPROVAL: July 1, 2005

ACKNOWLEDGMENTS

I wish to express my gratitude to my supervisor Assist. Prof. Murat Gülsoy. I want to thank him for his guidance, insightful comments, and helpful advice.

I would like to thank Murat Canpolat who improve CancerScanner system and make this study possible. I could not achieve this work without his support.

I want to thank Assist. Prof. Ata Akın for not only being a member of my thesis committee but also his encouraging guidance, support and also his valuable contributions to this study.

I would like to thank Assist. Prof. Can A. Yücesoy for being a member of my thesis committee and his valuable suggestions.

I also want to thank my colleagues; Özgür Tabakoğlu and Özgüncem Bozkulak who were extraordinarily helpful during this work.

This study was supported, in part by Bogazici University Research Fund under Grand 04X101 to Murat Gülsoy.

I am grateful to my family for their support.

I am very grateful to Bülent Hoca for his love and patience during this work.

ABSTRACT

CANCER DIAGNOSIS VIA ELASTIC SCATTERING SPECTROSCOPY

The goals of this study were to test the reliability of CancerScanner system whether it can detect the optical alteration of tissue dependent on temperature and to test the system on human tissues in which system can detect the cancerous lesions and examine the efficiency of this system. Cancerous tissue shows morphological alterations in the cellular level. Such changes may be detected by using the spectrum of the light scattered back from the tissue. Cell nuclei may be modelled as Mie particles that are larger than the wavelength of illuminating light. CancerScanner system is based on Mie theory and it uses elastic scattering spectroscopy method to differentiate cancerous tissue. This system delivers and detects white light with single optical fiber. The scattered light from tissue is detected by a spectrometer and spectrum is analyzed in PC with software. In this thesis work firstly CancerScanner system reliability was tested on lamb brain tissues *in vitro*. Tissues were coagulated at different temperatures and elastic scattering spectroscopy (ESS) spectra were taken from native and coagulated tissues. It was observed that as the coagulation temperature was increased, the slope of the elastic scattering spectra decreased. This showed that the slopes of ESS spectra taken with CancerScanner system in the visible range give valuable information about alterations of tissue optical properties. Secondly, the system was tested on human tissues *in situ*. The diagnostic efficiency of CancerScanner system was 86.6 % for lung tissues and paratracheal lymph nodes, and 80 % for brain tissues in differentiating cancerous and normal tissues. The system could not differentiate fat from tumor therefore; it was not successful on detecting breast tumors.

Keywords: *Elastic scattering spectroscopy, optic cancer diagnosis*

ÖZET

ESNEK SAÇILIM SPEKTROSKOPİSİ İLE KANSER TEŞHİSİ

Bu çalışma; Kanser Tarama sisteminin güvenilirliğini, dokudaki sıcaklık değişimine bağlı optik değişiklikleri tespit edip edemediğine bakarak test etmeyi ve sistemin insan dokularında kanseri tespit edebilme başarısını test etmeyi hedeflemektedir. Kanserli doku hücresel düzeyde morfolojik değişiklikler göstermektedir. Hücrelerin bu değişimleri dokudan geri saçılan ışığın spektrumu yardımıyla tespit edilebilir. Gelen ışığın dalgaboyundan daha büyük olan hücre çekirdeği, Mie parçacığı olarak modellenebilir. Geliştirilen Kanser Tarama sistemi Mie kuramına dayanmaktadır ve kanseri tespit etmek için esnek saçılım spektroskopisi yöntemini kullanmaktadır. Bu sistem tek bir optik lif yardımıyla beyaz ışığı taşır ve dokudan geri saçılan ışığı toplar. Saçılan ışık spektrometreye gönderilir ve spektrum bilgisayarda yazılım aracılığıyla analiz edilir. Bu tez çalışmasında ilk olarak *in vitro* kuzu beyin dokusunda yapılan ölçümlerle Kanser Tarama sisteminin güvenilirliği sınanmıştır. Dokular farklı sıcaklıklarda koagüle edilmiş ve doğal dokular ile koagüle edilmiş dokuların esnek saçılım spektroskopisi (ESS) spektrumları alınmıştır. Koagülasyon sıcaklıkları arttıkça esnek saçılım spektrumlarının eğimlerinin azaldığı gözlenmiştir. Bu, Kanser Tarama sistemi ile alınan ESS spektrumlarının eğimlerinin dokuların optik özelliklerindeki değişimler hakkında kesin bir bilgi verdiğini göstermiştir. Daha sonra sistem *in situ* insan dokularında denenmiştir. Kanser Tarama sisteminin kanseri teşhis etme başarısı akciğer ve paratrakeal lenf nodları için % 86.6, beyin dokuları için ise % 80'dir. Sistem yağ dokusunu tümörden ayırt edememiştir bu nedenle meme tümörlerini teşhis etmede başarısız olmuştur.

Anahtar Sözcükler: *Esnek saçılım spektroskopisi, optik kanser teşhisi*

TABLE OF CONTENTS

LIST OF FIGURES

LIST OF TABLES

LIST OF ABBREVIATIONS

ESS	Elastic Scattering Spectroscopy
MRI	Magnetic Resonance Imaging
LASER	Light Amplification by Stimulated Emission of Radiation
UV	Ultraviolet
NAD(P)H	Reduced Nicotinamide Adenine Dinucleotide Phosphate
FAD	Flavin Adenine Dinucleotide
IR	Infrared
mm	Millimeter
cm	Centimeter
LSS	Light Scattering Spectroscopy
PESS	Polarized Elastic Scattering Spectroscopy
μm	Micrometer
nm	Nanometer
FDTD	Finite Difference Time Domain
NA	Numerical Aperture
PC	Personal Computer
a.u.	Arbitrary Unit

LIST OF SYMBOLS

λ	Wavelength
I_b	Intensity of ESS spectra taken from black flat container
I_s	Intensity of ESS spectra taken from Spectralon
I_t	Intensity of ESS spectra taken from tissue
I_c	Intensity of correlated spectrum
ºC	Degree Celsius

1. INTRODUCTION

1.1 Motivation and Objectives

In recent years optical methods have become an important research area in tissue diagnostics [1]. These techniques attempt to diagnose diseases less painfully and non-invasively. Diagnoses of diseases earlier, cheaper and with real time methods are other aims of these studies such as optical imaging and spectroscopy.

Neoplasm is an autonomous growth of tissue. Cancer which is a genetic disease is synonymous with malignant neoplasm. There are several methods in cancer diagnosis. Most cancers are diagnosed histopathologically by phenotypic markers, such as nuclear to cytoplasmic ratio, appearance of cell nuclei [2]. Surgical removal of the tissue is needed for this histological examination. This may be possible mostly after cancerous lesions become large and such biopsy procedure is painful, time consuming, and risky (e.g. due to anesthesia, inflammation) for the patient [3]. However, cancerous lesions may be differentiated from healthy tissue with optical methods according to the structural alterations. More than 85% of human cancers originate in the epithelial tissues [4]. It is also known that nuclei of many types of cancerous and precancerous cells are significantly larger than nuclei of normal cells [5], nuclear to cytoplasmic ratio and chromatin texture of cancerous cells are different from normal cells. These morphological changes affect the optical properties of tissues and allow cancer diagnosis using optical methods.

Various spectroscopic methods can be used to detect changes in molecules or cells such as diffuse reflectance spectroscopy, fluorescence spectroscopy, and elastic light scattering spectroscopy. While the biochemical information can be obtained by measuring absorption, Raman scattering, or fluorescence signals, the structural and morphological information may be obtained from elastic scattering properties of tissues.

Light is scattered and absorbed in turbid media due to inhomogeneities and absorption characteristics of the medium. Light scattering can be used to diagnose precancerous lesions at histologically-detectable stages. Biological tissue is a turbid optical medium; such light transport is dominated by elastic scattering. The mitochondria and other intracellular substructures that scatter the light have smaller dimensions than visible wavelengths. Larger structures such as cell nuclei also scatter light [7 - 9]. Recent

studies [6, 7] were focused on measuring the size of the cell nuclei by light scattering spectra in ultraviolet and visible scale. These studies showed that the cell nuclei can be modeled as spherical Mie objects and their size distribution can be determined from the dependency of back-scattering light on the wavelength. Scattering by a particle with dimensions larger than the visible wavelength like nucleus can be described by Mie theory [10-12]. A recent study [13] shows that the elastic scattering spectrum of particles in different diameters has a distinct oscillatory pattern in visible wavelength region. Each pattern may be thought as a signature of the size of the particles. Particle size is approximately a linear function of the total number of maxima and minima. A three-dimensional computation study [14] showed that wavy pattern of scattered light disappears if light is scattered by not only the nucleus but also by other organelles.

The design of fiber-optic probes plays an important role in optical spectroscopic studies. Canpolat and Mourant [13] described an *in situ* technique to determine scatter with a single-fiber optic probe. CancerScanner system [15] uses a single optical fiber for both delivering white light and collecting scattered signal. This system uses the elastic scattering spectroscopy (ESS) signal to distinguish cancerous lesion from normal. In an animal study using this system, ESS spectra of normal tissue was shown to have positive slope whereas, cancerous tissue yielded negative slope [15].

The goals of this work are:

1) to test the reliability of the CancerScanner system whether it can detect the temperature dependent alteration of tissue

2) to test the CancerScanner system on different human tissues and examine its success rate in detecting of the cancerous lesions.

1.2 Outline

In Chapter 2, an introduction is presented on cancer, cancer diagnosis methods, and optical spectroscopic approaches for tissue diagnosis, and studies on elastic light scattering spectroscopy in cancer diagnosis.

Chapter 3 gives a description of CancerScanner system that is used in this study. Also calibration of the system is described.

In vitro study on lamb brain tissue with CancerScanner system and its results are given in Chapter 4.

In Chapter 5, the results of *in situ* measurements on different human tissues are found. The success of the CancerScanner system is discussed briefly.

Chapter 6 gives the general conclusions of this study.

2. BACKGROUND

2.1 Cancer

Humans have been plagued by many different diseases during the whole of the history of civilization. In ancient times leprosy was dreadful, in Middle Ages and Renaissance the frightening disease was Black Death (bubonic plague). In the 20th century, infectious diseases remained the major mortality risk to the cancer [16, 17]. Cancer is not the disease of this century but the public became aware of its significance in the 20th century.

There are 20 millions of people suffering from the cancer and every year 150-300 of each hundred thousand people is getting cancer in the world. In Turkey a hundred and fifty thousand people get cancer every year. Cancer became the second most common cause of deaths (15%) in 1998 after the cardiovascular diseases (38%). Parts of the body that cancerous lesions mostly occur (Table 2.1-2.2) are breast, lung, stomach, skin, uterus, and prostate [18].

Table 2.1
The most common 5 cancerous types that are frequently seen in women in Turkey according to various sources [18]

Cancer Region	All Hosp. [1] (%)	Ministry of Health[2] (%)	Pathology Centers[3] (%)	KIDEM[4] (%)
Breast	14,9	23,3	22,6	26,7
Uterus	10,7	-	-	6,5
Lung	7,2	3,9	-	-
Cervix	-	-	3,7	5,9
Stomach	6,8	6,7	3,6	-
Lymphoma	6,7	-	-	-
Over	-	5,1	-	6,4
Skin	-	-	20,3	-
Soft tissue	-	-	3,7	-
Colorectal	-	3,9	-	5,9

[1] According to patient records from all hospitals in Turkey in 1994
[2] According to (1996) data of Ministry of Health of Turkey, Department of Cancer Control
[3] According to records of 16 pathology centers for six years
[4] According to (1993-1994) records of Izmir Cancer Watch and Control Center

Table 2.2
The most common 5 cancerous types that are frequently seen in men in Turkey according to various sources [18]

Cancer Region	All Hosp.[5] (%)	Ministry of Health[6] (%)	Pathology Centers[7] (%)	KIDEM[8] (%)
Lung	27,7	25,7	-	38,6
Stomach	8,5	8,3	6,1	5,2
Lymphoma	7,4	-	-	-
Prostate	6,3	4,0	-	-
Larynx	6,4	6,0	7,8	6,9
Skin	-	-	22,6	-
Bladder	-	6,6	7,4	6,8
Oral Cavity	-	-	5,7	-
Colorectal	-	-	-	4,5

The word tumor means literally a swelling, independent from its cause. The medical term used for cancer or tumor is neoplasm. A neoplasm is a heritably altered, relatively autonomous growth of tissue. A malignant neoplasm is synonymous with cancer. Tumor is a general term indicating any abnormal mass or growth of tissue.

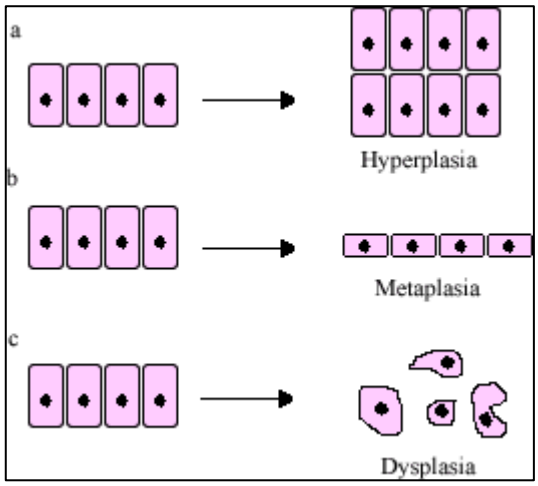

Figure 2.1 Hyperplasia, metaplasia, and dysplasia [19]

Hyperplasia (Figure 2.1.a) is an abnormal increase in cell associated with relatively normal tissue organization. Pathologic hyperplasia may be a step in the development of neoplasia (cancer). Thus hyperplastic changes in some tissues may be considered pre-malignant. Metaplasia (Figure 2.1.b) is a change in cell structure from one fully differentiated form to another and it represents an attempt by tissue to replace

[5] According to (1996) data of Ministry of Health of Turkey, Department of Cancer Control
[6] According to records of 16 pathology centers for six years
[7] According to (1993-1994) records of Izmir Cancer Watch and Control Center
[8] According to records of 16 pathology centers for six years

a susceptible cell type with a more resistant one. Like hyperplasia it may be considered a pre-malignant change. Dysplasia (Figure 2.1.c) is disordered cellular morphology, organization, and function. It is always associated with pathologic process. Dysplastic tissues display abnormal variation in overall cell size and shape as well as nuclear structure. Cell numbers are typically increased in dysplastic tissue and normal tissue morphology is distorted. It is strongly implicated as a precursor to cancer. Dysplasia is distinguished from cancer by the important fact that dysplasia is reversible. Unlike cancer cells, dysplastic cells are not autonomous - they are still capable of responding to normal physiologic growth and differentiation controls.

Carcinogenesis, the process by which cancers are generated, is a multi step mechanism resulting from the accumulation of errors in vital regulatory pathways. Cancers are most common in epithelial cells. It is initiated in a single cell which then multiplies and acquires additional changes that give it a survival advantage over its neighbors. The generation of these errors and cell multiplying take time. Cancers continue to change their behaviors as they progress [20].

An oncogene is a gene that can cause a cell to develop into a tumor cell. Tumors arise from the concerted action of a number of oncogenes [21]. The protooncogene is a gene that is involved in signal transduction and execution of mitogenic signals. Protooncogene can become an oncogene by a modification of its original function. It can be activated by a mutation so the protein structure of it changes. These altered cells must be amplified to generate billions of cells that constitute a cancer. Cell proliferation is a core feature of cancer. Other important feature is that cancer cells have a degree of autonomy. While normal cells are subject to internal and external inhibitor signals, this is lost during carcinogenesis. Degree of autonomy varies. While contact with extracellular matrix is growth inhibitory for normal cells, cancer cell proliferation increases. [20]

The cancer development may be viewed as:

Normal → Hyperplasia → Carcinoma in situ (localized) → Invasive cancer (surrounding) → Metastatic cancer (remote tissue)

Increased cell mass may be considered benign not a cancer and its growth may be controllable. Additional changes enable those cells to invade the surrounding tissue and metastasize to other parts of the body. This invasion ability of cancer cells reflects membrane modifications resulting in diminished cell to cell interaction [20].

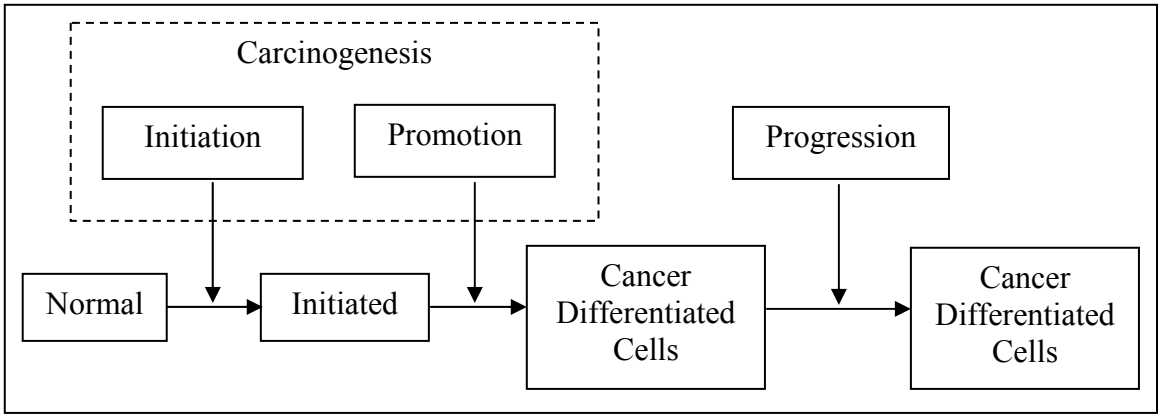

Figure 2.2 Initiation, promotion, and progression of cancer

Neoplastic development begins with initiated cell resulting from the administration of an initiating agent (carcinogen). It is followed by promotion to a visible tumor and progression of this neoplasm to the malignant or cancerous state (Figure 2.2).

2.2 Cancer Diagnosis

Cancer is diagnosed clinically at an advanced stage -in progression rather than carcinogenesis. Growth detection according to clinical symptoms may be very late. Tumor passes the halfway stage in its life (Figure 2.2). Tumor can be detected by X-ray when it is smaller or some symptoms, for example the presence of hemoglobin in faeces for colon cancer, can let earlier detection.

Tumors may be detected from clinical symptoms and by imaging methods. X-rays, tomography, ultrasound, or MRI (magnetic resonance imaging) can be used as imaging methods according to tumor area for diagnosis or to determine its size and location. However location information is usually not precise.

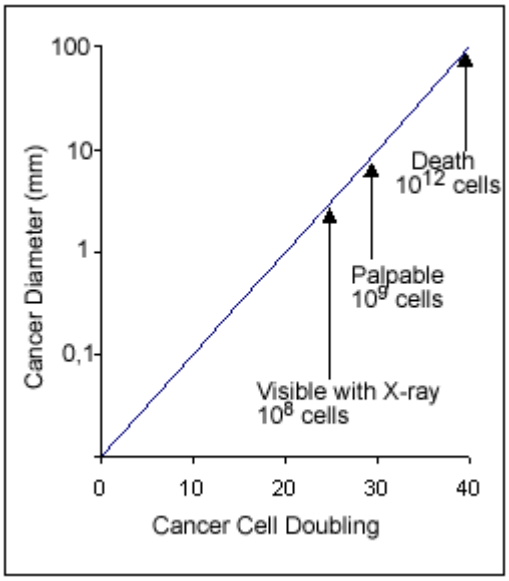

Figure 2.3 Relationship of clinical symptoms to cancer size [20]

Biopsy particle is taken or whole tumor is dissected with surgical operation after the tumor is detected. The part extracted is examined pathologically. Pathology defines the type of cancer and also if the neoplasm is benign or malignant.

Three types of pathology are defined according to what is analyzed. They analyzed intact tissues, individual cells, or chemical analysis of body fluids. Cancer is the growth of one or a few cell types and this differential growth disrupts the normal interrelationships between the different cell types and the extracellular matrix. These features can be examined histopathologically by microscopic image of stained tissue sections. Cytology deals with single or small group of cells removed from a suspect site. Chemical pathology analyzes the tissue, blood, or urine chemically.

Histopathology is the routine method for characterizing an excised tumor. Diagnosis relies on the appearance of the cells and also on the tissue architecture (Neoplastic cell relationship to the extracellular matrix and other cells) [20]. The main features that distinguish an epithelial cancer from its normal are (Figure 2.3): cell and nuclear shape changes, nucleolus enlargement, altered ratio of epithelium/stroma, basement membrane disappearance.

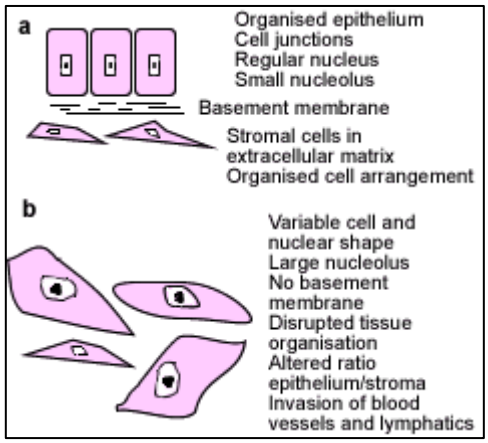

Figure 2.4 Features of epithelium that distinguish normal tissue (a) from a cancer (b)

Structurally, some of the diagnostic features of malignant cells as defined by cytologists are: (1) increased nuclear/cytoplasmic ratio; (2) increased nucleolar/nuclear ratio; (3) enhanced nuclear staining; and (4) increased incidence of mitotic figures and the presence of abnormal mitoses [16].

2.3 Optical Spectroscopy in Cancer Diagnosis

More than 85% of cancers arise in epithelial tissues. The majority of epithelial cancers are preceded by precancerous changes that affect both the surface epithelium and deeper stroma [4].

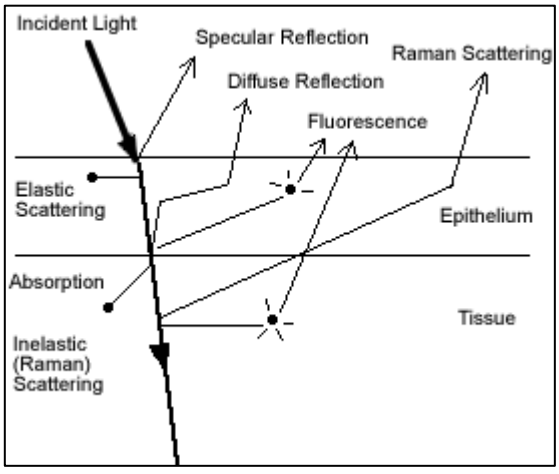

Figure 2.5 Schematic diagram of light pathways in tissue

When a beam of light reaches the surface of the tissue, (Figure 2.4) part of it will be reflected by the surface directly, the rest will refracted and transmitted into the tissue. The transmitted light is scattered and absorbed by the tissue. Tissue optical

properties can be used for determining the structural features, biochemical composition, and functional changes in normal and abnormal tissues. [22]

There are ongoing studies on various spectroscopic techniques which are uses the reflectance of light from tissue, fluorescence properties of tissues, and Raman scattering properties (Figure 2.4) in tissue diagnostics.

Many studies give attention to biochemical tissue analysis by various types of fluorescence spectroscopy. Fluorescence spectroscopy can be used to examine chemical composition of materials such as tissue [23]. Using different excitation wavelengths and analysis techniques laser induced or non-laser based –UV excitations-fluorescence spectroscopy can be used for detection of malignant or pre-malignant tissues in a variety of organ systems. Pre-cancers are characterized by increased metabolic activity, which affects mitochondrial fluorophores NAD(P)H and FAD, and changes the fluorescence properties of tissue. When molecules in tissues are stimulated by light, they respond by becoming excited and re-emitting light of varying colors (fluorescence) that can be captured and measured by sensitive optical equipment. Fluorescence spectroscopy is based on the fact that different metabolic states and biochemical components emit light differently. This provides information about the chemical composition of the tissue, about molecular and biochemical changes, as a function of the stages of disease.

Most endogenous fluorophores are involved in cellular metabolic processes. Collagen and elastin are the most important structural fluorophores and their composition involves cross linking between fluorescing amino acids. The fluorescence properties of tissue is determined by the concentration of these fluorophores, the distinct excitation and emission spectrum of each fluorophores, distribution of various fluorophores in the tissue, the tissue architecture and the wavelength dependent light attenuation due to the concentration [22]. Regardless of tissue types, malignant tissues typically exhibit lower fluorescence emission intensities compared to their corresponding normal tissues at specific excitation wavelengths as reported for lung [24], esophagus [25], mouth [26, 27], nasopharyngeal carcinoma [28] and skin [23].

Transmitted light is absorbed and scattered by tissue. After multiple scattering, some of the transmitted light emerges again through the surface (Figure 2.4). This is

called diffuse reflection. The amount of diffuse reflection is determined by both scattering and absorption properties of the tissues. When the absorption is stronger the diffuse reflection gets less. Diffuse reflection gets larger if the scattering is stronger. For diagnostic purposes, the diffusely reflected light from tissue may be measured to probe the metabolic, physiologic, or possibly the structural status of the tissue [1]. In diffuse reflectance studies on tissue usually use the spectral region from about 600 to 1300 nm. At these wavelengths the absorption of light by most of soft tissues is a minimum. At shorter wavelengths in the ultraviolet region absorption is high due to specific chromophores such as melanin, hemoglobin. At longer wavelengths in the infrared (IR) region the water absorption is high. This region from red to near infrared - that relatively low absorption is seen in, is called 'therapeutic window'. It allows penetration of light into tissue and high remittance of light scattered out of the tissue (diffuse reflectance) after deep penetration.

Diffuse reflectance spectroscopy estimates optical coefficients of tissue in optical biopsy. Wavelength dependence of reduced scattering coefficient can be measured by diffuse approximation. The diffusion approximation is used to analyze diffuse back-reflected light with estimated optical coefficients of tissue that are correlated to physical structure and chemical composition of the tissue. The distance between source and detector fiber should be 3-4 millimeters for tissue diagnosis. The sampled volume should be large enough i.e. ~1 cm when using this technique [15].

2.3.1 Elastic Light Scattering

Interaction of light with matter leads to change of the direction and/or the length of the incident light wave. This is called scattering. The incident light is deflected by collisions with particles or centers of inhomogenity of the medium. A perfectly homogenous medium cannot change the direction of photons. Scattering of light occurs as an effect of heterogeneity in optical properties of the medium. Absorption is the transformation of the light energy to some other form of energy. Scattering is usually accompanied by absorption. The scattering events in an optically turbid medium such as tissue change the direction of light propagation and cause attenuation of the light traversing the medium. The process of scattering depends on the light wavelength and on the scattering medium properties; especially on the size and the density of the medium, and the state centers (particles) of inhomogeneity.

Cells and tissues have a complex structure. Subcellular organelles are not uniform and have complex structures and shapes. They can be referred to as scattering particles [29].

When the scattering events change only the direction of the photon propagation, elastic light scattering occurs. The photon energy and the frequency of the initial light wave are preserved. This type of scattering occurs in light scattering by static objects when the density inhomogeneities do not propagate [11, 30].

2.3.2 Mie Theory

Many cell organelle structures are small compared to wavelength. Light scattering by such particles is known as Rayleigh scattering. It refers to the scattering of light from particles up to about a tenth of the wavelength of the light. Rayleigh scattering is more effective at short wavelengths as the intensity is in reciprocal to the fourth power of the wavelengths. Rayleigh scattering is characterized by a broad angular distribution and the scattering cross-section dependence on the particle's linear dimension on light wavelengths λ as $1/\lambda^4$ [31].

When the diameters of scattering spheres like a cell nucleus are very large compared to the wavelength of the scattered radiation, the Mie theory must be applied to obtain an accurate prediction of scattering. The exact solution of the scattering of a plane electromagnetic wave by an isotropic, homogeneous sphere was obtained by Mie in 1908 and is usually referred to as the Mie theory [10-12]. In comparison with the Rayleigh scattering, in Mie theory the scattered light is not strongly dependent to the wavelength. The Mie scattering on particles larger than the wavelength is mostly forward-directed.

It is known that scattering by homogenous spheres that contain isotropic dielectrics can be analyzed by Mie theory. However the scattering properties of most particles such as cells that have neither exact spherical shapes nor homogenous compositions cannot be obtained analytically [32]. The new methods are needed to compute the scattering patterns of heterogeneous organelles.

2.3.3 Cancer Diagnosis via Elastic Light Scattering Spectroscopy

Optical spectroscopy has the potential to provide diagnostic information as mentioned before. When elastic scattering spectroscopy (ESS) is employed for tissue diagnosis, the optical alterations of tissue are detected and diagnosed using spectral measurements of the elastic scattered light, in a manner that is sensitive to both scattering and absorption properties of the tissue, over a wide range of wavelengths.

The technique that is sensitive to the wavelength and angle dependence of scattering and absorption bands is based on the fact that many tissue pathologies including a majority of cancers, show morphological changes at the cellular and sub-cellular level. Pathologists examine the tissue histopathologically. Microscopic examination of the cell architecture or morphology is based on the sizes and shapes of cells, the ratio of nuclear to cellular volume, the form of the bilipid membrane, gathering patterns, etc. The intent of the ESS approach is to generate spectral signatures of relevance to the tissue parameters that histopathology address [3].

While the photons returned after multiple scattering events produce the diffuse reflectance the photons returned after a single scattering in the backward or near-backward directions produce a single-scattering component. The diffusive component contains information about tissue scatterers and absorbers. The single-scattering component is sensitive to morphology of the upper tissue layer that is limited by the epithelium. The single-scattering component is more important in diagnosing the initial stages of the epithelial precancerous lesions. The major advantage of ESS in cancer diagnosis is its sensitivity to the structural information of tissues and cells [33]. The wavelength dependence of light scattering is sensitive to the morphology of light scatterers [34]. The morphological structure alterations lead to changes in the elastic scattering signal.

There are different tissue diagnosis studies based on the light scattering spectroscopy. Whole size distribution studies referred cell nuclei as Mie spherical particle. Some studies [14, 35] investigate computational methods in order to calculate the light scattering properties of cells over a range of wavelengths according to Mie calculations. Various experimental setups and measuring methods are examining with light scattering spectroscopy (LSS). Some studies report an *in situ* method with polarized light. These studies observe the spectrum of polarized back-scattered light from turbid sample [33],

normal human colon, and tumorous colon tissue [5, 36, 37], and bladder [33]. While the advantage of polarized elastic scattering spectroscopy (PESS) is its stronger sensitivity to morphological changes in tissue, the disadvantage of these systems is their complexity. The complex device and fiber optic probe design of PESS is in the early stage of development.

Other method for determining the size distribution of cell nuclei with LSS is angle-resolved low-coherence interferometry [8]. This *in situ* technique measures scattered light as in flow cytometry. The information about cellular organization and substructure is obtained by examining the spatial correlations within the monolayer. The disadvantage of this system is long data acquisition times. A new system is developed to improve data acquisition and analysis times [9].

2.3.4 Single Optical Fiber

Another difference of the LSS systems is their light delivery and collection design. PESS systems generally use lenses and beam splitters to deliver light to the tissue or tissue phantom and collect scattered light. Other studies use different type of optical fibers.

The design of fiber-optic probes has an important role in optical spectroscopic studies. It can affect the origin of collected light and the collection efficiency -total number of photons collected vs. total number of photons launched. Spectroscopic techniques often use optical fiber probes since they allow for flexible delivery and collection of light even in hard to reach anatomical sites. Precise targeting of specific tissue areas and identification of the origin of optical signal affects the diagnostic value of optical spectroscopic techniques [38].

When using two fibers -one is from light source to tissue, other is from tissue to detector- the spectral dependence of the collected light is insensitive to the size and shape of scattering centers if two fibers are separated from each other over than 0.5cm [3].

Single optical fibers have been commonly used as light delivery and collection tools for optical diagnosis. It is observed that single fiber probes exhibited higher depth sensitivity [38, 39]. Changes in tissue optical properties affect single-fiber measurements. When a single optical fiber is used, two factors affect the measurement of collected light:

- The light transport in the medium that describes the amount of light that returns to the fiber

- The light coupling to the optical fiber that depends on the angular distribution of photons entering the fiber [40].

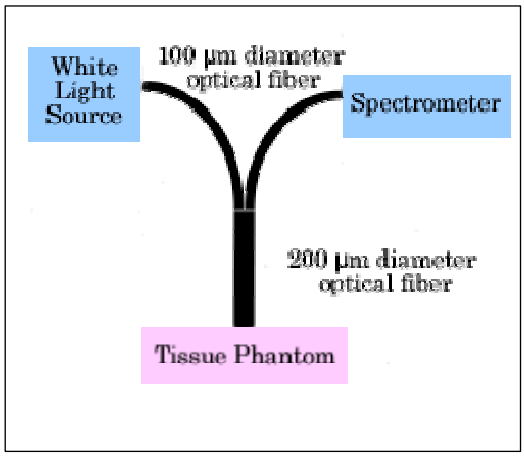

Figure 2.6 Measurements with single optical fiber

To reduce the contribution of multiple scattered light probe geometry is important. A single optical fiber can optimize the detection of singly scattered photon. The single fiber is more sensitive to backscattering from small depths that increase the probability of measuring singly scattered light from epithelial layer [41, 42].

Canpolat and Mourant [13] designed a single optical fiber to determine the particle size of turbid media (Figure 2.5). They used single optical fiber to deliver and detect white light in contact with the medium. The major advantage is the decreased depth of light penetration. Most cancers originate in epithelial tissue that is only a few hundred micrometers thick. Consequently, it is desirable for most of the scattering events of the collected photons to take place within 500 µm of the surface as is the case in a single-fiber measurement. Another advantage of a single fiber is the reduced interference of absorption in the measurement of scattering properties. This single fiber diameter is only 0.2 mm. It has many other advantages. The probe can fit into endoscope channels easily, a quite small volume can be probed and measurements can be taken locally.

2.3.5 Particle Size Analysis

In situ technique was described to measure scatter size with white light ESS [13]. In measurements a white light source, a single optical fiber for delivery of light and collection of scattered light from polystyrene particles in different diameters, a spectrometer, and a PC to analyze the spectrum were used. This study indicated that the ESS spectrum of each size (0.329, 0.451, 0.890, and 2.020 μm) of a sphere has a distinct oscillatory pattern (Figure 2.6). Each pattern can be thought as a signature of the size of the particles.

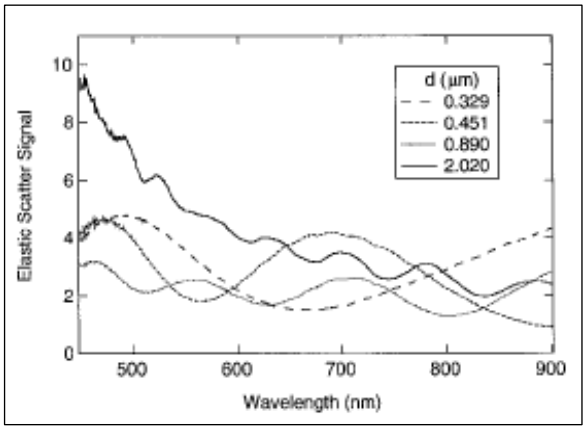

Figure 2.7 Elastic scatter spectra of tissue phantoms. Diameters of the polystyrene particles are 0.329, 0.451, 0.890, and 2.020 μm. Reduced scattering coefficient is 1.5 mm^{-1} at 633 nm [13]

When the experiments were repeated with a reduced scattering coefficient, 0.75mm^{-1}, (previous one was 1.5 mm^{-1}) it means that the concentration of the particles is two times lower than in the first tissue phantom, there was a little difference in the oscillation pattern of spectra from tissue phantoms with the same size.

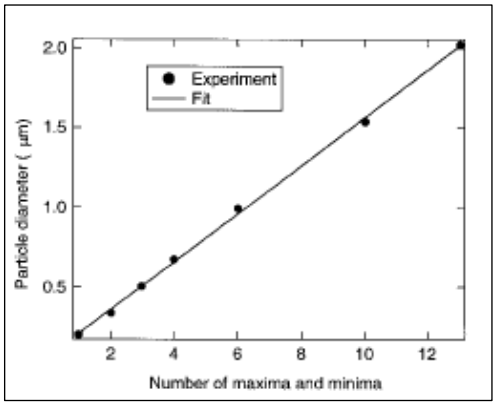

Figure 2.8 Particle diameters as a function of the total number of maxima and minima of the derivatives of the ESS in wavelength range 450-800 nm [13]

When the derivative of the spectra (Figure 2.6) is taken, it is observed that the frequency of oscillations increases with particle size. The number of the maxima and minima in the 450-800 wavelength range provides information about diameter of the particles. Particle size is approximately a linear function of total number of maxima and minima (Figure 2.7).

To understand the effect of the refractive indices change of the scatterer, the polystyrene spheres were immersed in optical couplant instead of water. The large change in refractive indices 1.20 to 1.09 affects the spacing between adjacent maxima of the oscillations in the derivative spectra. It was observed that 1% change in refractive index causes a 1% change in spacing. It was estimated that this difference would cause an error of approximately 8 nm in size determination.

2.3.6 Calculating Light Scattering from Biological Cells

Mie theory has been used to approximate tissue scattering at cellular level with the assumption that cells are homogeneous spheres of a single size. However, individual cells have complex structures containing many organelles. Mie theory can describe the scattering of light from spherical organelles such as nucleus that has larger diameter than visible light but it can not account for a combination of organelles within a cell. In recent studies [14, 35], two- and three-dimensional scattering patterns of cells were computed by using the finite-difference time-domain method. These studies modeled light scattering from cells containing multiple organelles (Figure 2.8). The FDTD technique is a potent computational method that is a full vector, 3-D solution of Maxwell's equations.

It was observed that the geometry chosen significantly impacts scattering properties. Scattering of light from nucleus only, cell with mitochondria, and cell with melanin has different patterns. The results of these studies showed that the wavy pattern of scattered light disappears if light is scattered by not only nucleus but also by other organelles.

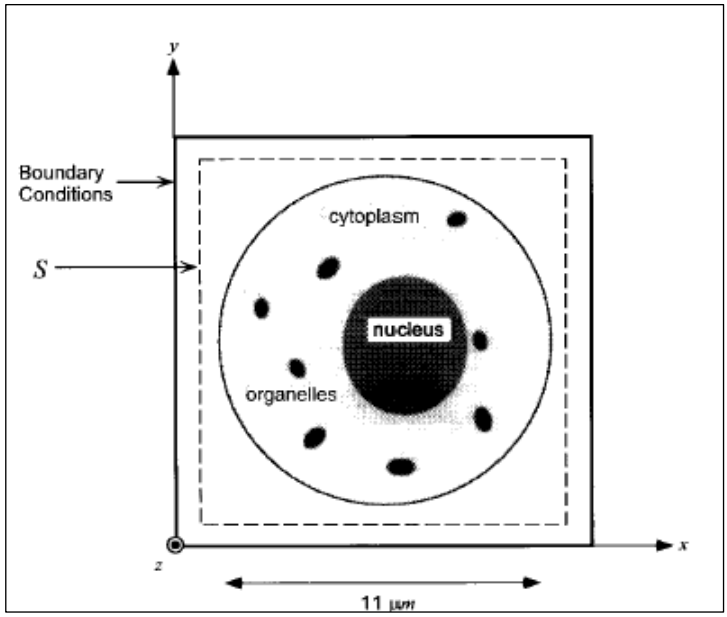

Figure 2.9 Geometry of the FDTD simulation demonstrating how the cell is constructed by assigning each component a different index of refraction [14]

In the study of R. Drezek et. al. [35], heterogeneous normal and pre-cancerous cervical cells were modeled with pulsed FDTD method. In the simulation intensity of the scattered light was integrated as a function of wavelength for different angular ranges in the light range of 600-1000 nm. In the angular range of 160-180 degrees the difference between the intensities of pre-cancerous cells and normal cells is the most dominant. The intensity of scattered light from normal cells increases with wavelength and does not change for dysplasia in this wavelength range (Figure 2.9).

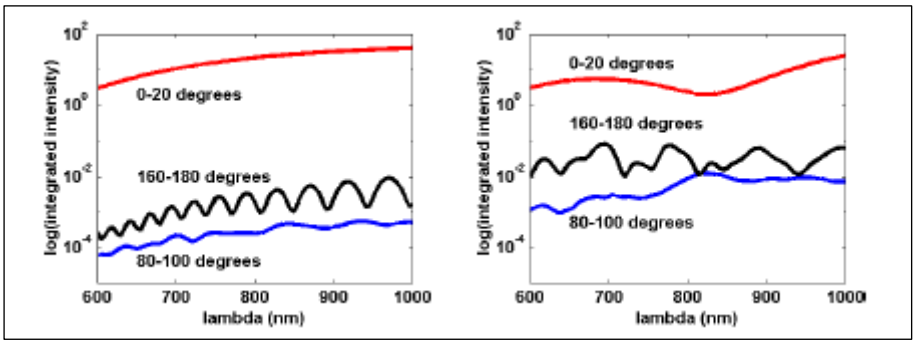

Figure 2.10 Scattering from normal (left) and dysplastic cell (right) [35]

2.3.7 CancerScanner System in Animal Study

Elastic-scattering spectroscopy (ESS) spectra were used to differentiate cancerous and normal breast tissues in mice *ex-vivo* with CancerScanner system [15].

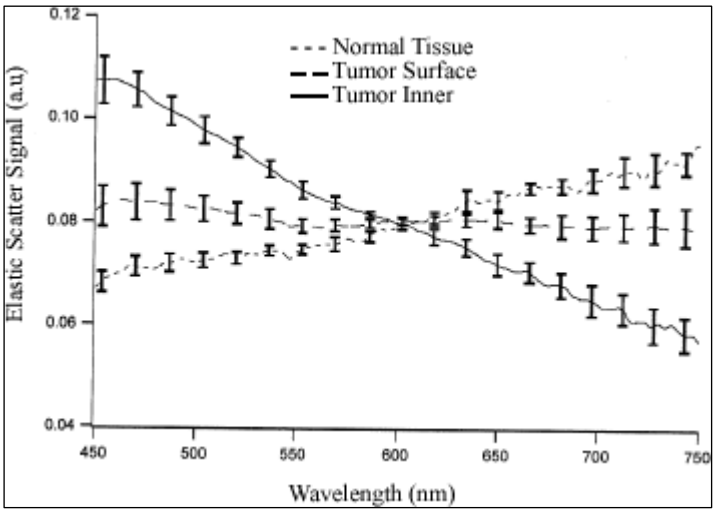

Figure 2.11 A graph of the light scattering spectra scattered back from epithelial tissue of mouse breast and from the tumor. The slope of the spectrum from normal tissue is positive and that from tumor is negative [15]

In the study of Canpolat et. al. [15] it was observed that there were no oscillations on the spectra of normal and cancerous cells. This is consistent with poly-dispersed nature of the scatterers' size in tissue.

It was also observed that slope of the spectra of epithelium tissue was positive whereas that of cells inside the tumor was negative (Figure 2.11). Slope of the spectra taken from surface of tumor was nearly zero this was due to the average spectrum taken from both cancerous and normal cells at the membrane. Spectra taken from inside and surface of the tumor are similar: they are both negative. These results are consistent with the results of R. Drezek et. al. which was previously mentioned [35].

3. MATERIALS AND METHODS

3.1 System

In CancerScanner system a tungsten lamp (Ocean Optics, Inc. Florida, USA) is used as the light source. Optical fibers are used to deliver light to and from the tissue (Figure 3.1). Both of them are 100-µm in diameter and the probe tip is 200-µm. Two optical fibers were butted up against the 200-µm fiber in an SMA barrel connector. They have numerical aperture of 0.22, and a length of approximately 100-cm. When single optical fiber measurements are performed on scattering samples, the specular reflection of launched that is due to the index of refraction mismatch between the optical fiber and the sample is an important fraction of the signal. For that reason, the fiber has to be polished and cleaned carefully. In CancerScanner system the tip of the fiber was polished at an angle of approximately 50º instead of the sharpest angle in the probe tip 90º to avoid specular reflection. The spectrometer (Ocean Optics, Inc. Florida, USA) is connected to a PC and the elastic scattering spectra of tissues are taken and analyzed by the software (Ocean Optics, Inc. Florida, USA).

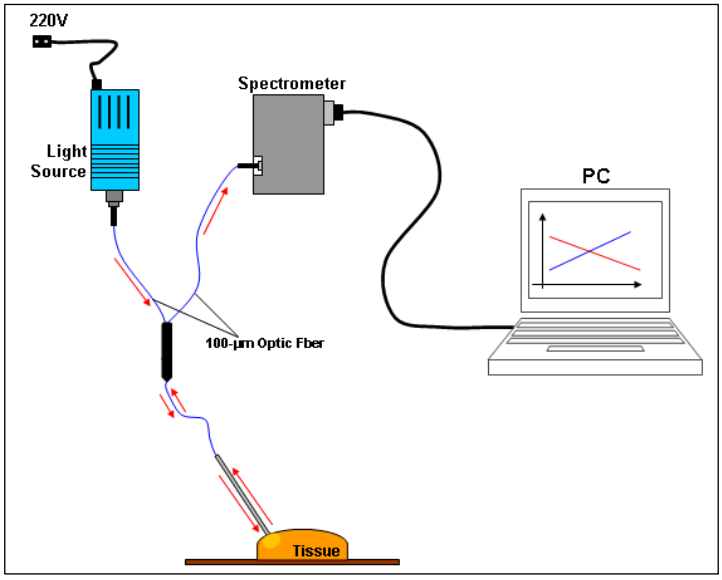

Figure 3.1 CancerScanner System Setup: Light is delivered from a small white light source to the target by fiber optics. The 100-µm optical fiber from the lamp is butted to a 200 µm fiber that is in contact with the tissue. The collection path is from 200-µm through 100-µm fiber to the spectrometer. Spectrometer is connected to the PC

3.2 Calibration

In the measurements after the light source is turned on the tip of the probe is touched to the tissue and the scattered light spectrum is monitored by the interface (OOIBase32Platinum Ocean Optics, Inc, Florida, USA) on PC screen. To eliminate the background caused by the light source scattering from coupler and water from wet tissue system is needed to calibration. Firstly the spectrum is taken from water in a flat-black container (I_b) (Figure 3.2).

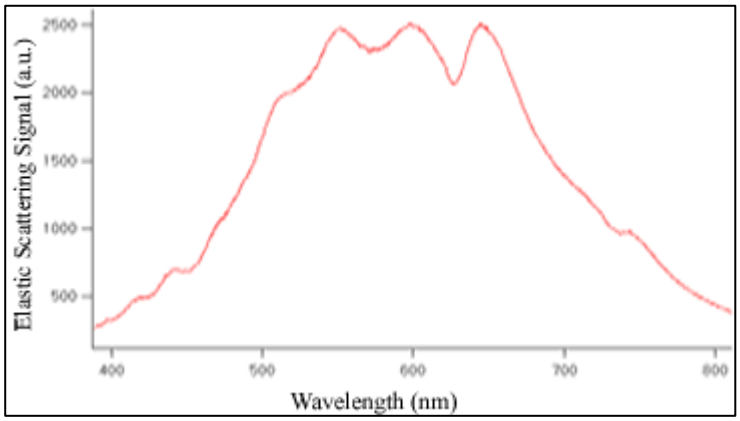

Figure 3.2 ESS spectrum from water in the flat-black container

Then it is taken from Spectralon (I_s) (Lab-sphere, Inc., North Sutton, N.H.) in water (Figure 3.3) with the probe not in contact with Spectralon.

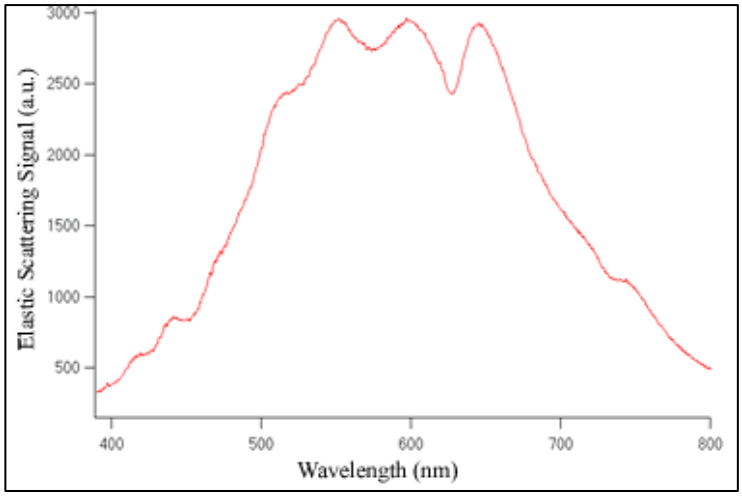

Figure 3.3 ESS spectrum from water in Spectralon (in the flat white container)

After taken spectrum from Spectralon calibrated transmission signal is taken (Figure 3.4) while the probe is still in the white container.

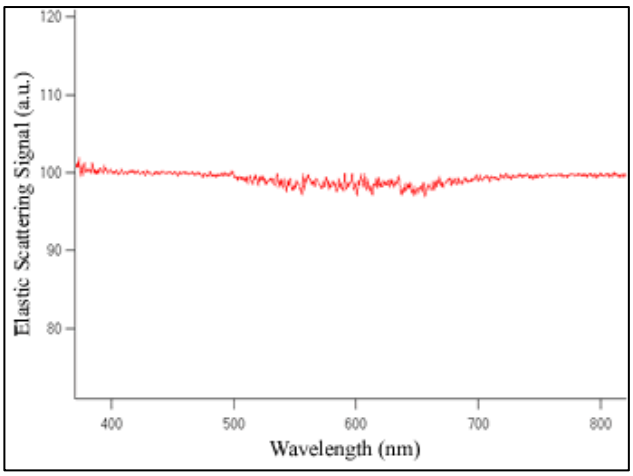

Figure 3.4 ESS spectra from water in Spectralon after calibration

After all, a spectrum can be taken from tissue (I_t). The corrected spectrum (I_c) is:

$$I_c = \frac{I_t - I_b}{I_{s-} I_b} \qquad (1)$$

To control the calibration, the spectrum is taken from tissue phantom that is dense suspension of 2-µm in diameter polystyrene particles (Duke Scientific Corp. California, USA). The elastic light scattering spectrum of it (Figure 3.5) is compared with the known spectrum of the phantom that has particles in same size.

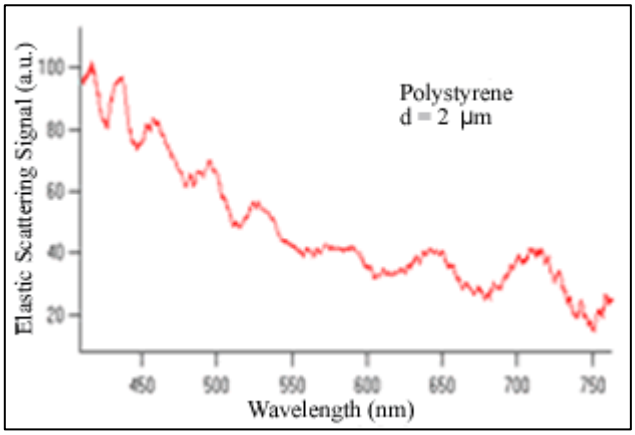

Figure 3.5 ESS of tissue phantom that contains polystyrene particles with the diameter of 2 µm

4. *IN VITRO* STUDY

Determining the optical properties of tissues is the main subject of various studies. The techniques are varying according to the purpose. One of these methods can be examining optical properties of the native and coagulated tissue. This is done in order to determine the efficacy of the laser procedure and the heat effect of laser on tissue. Therefore, this kind of studies uses different types of lasers that were developed according to clinical purposes [1, 43]. It is known from literature that the optical properties of tissues such as absorption and scattering coefficients change when coagulated. In this thesis, elastic scattering spectra of native and coagulated lamb brain tissues were taken in order to test the CancerScanner system if the graph of elastic scattering spectra that were taken from different parts of brain tissue changes when the optical properties of tissues changed. Also the differences and correlations between brainstem, cerebellum, gray matter, and white matter were examined according to their ESS spectra.

4.1 Method

Three lamb brains were used in this study. Parts of the brains; brainstem, cerebellum, frontal lobe gray matter, and frontal lobe white matter were sectioned and divided into small pieces. These four parts of the first lamb brain were coagulated at 45 ºC, the same parts of second brain were coagulated at 60 ºC, and the parts of third brain were coagulated at 80 ºC in heat block. Heat block temperature was constant during each coagulation process. Tissues were coagulated for 90 minutes for each temperature studied (45 °C ± 2, 60 °C ± 2, and 80 °C ± 2). Following coagulation, the elastic scattering spectra of each tissue were taken after CancerScanner system was calibrated (calibration procedure was described in chapter 3). Also the ESS spectra were taken *in vitro* from all three of the native lamb brains. At least ten elastic scattering signals were taken from each part of the tissues.

When analyzing the spectra of native and coagulated brain tissues, the slope of the wavelength versus elastic scattering signal was used in the visible wavelength range (450

nm to 750 nm). The slopes were normalized (x 10^6). Student t-test and correlation were used for statistical analysis.

4.2 Results

Figure 4.1 shows the plotted ESS spectra of native brainstem tissue as well as that of the tissues coagulated at 45 ºC, 60 ºC, and 80 ºC. The slope of the ESS spectra of native brainstem is 204.7 ± 2.46. The slope of the ESS spectra of brainstem that was coagulated at 45 ºC is 178.09 ± 2.44. While the slope of the ESS spectra of brainstem that was coagulated at 60 ºC is 55.342 ± 0.946, the slope of the ESS spectra of brainstem coagulated at 80 ºC is -60.383 ± 0.678. It is seen that as the coagulation temperature is increased the slope of the ESS spectra decreases from the relatively high positive values of native brainstem to lower positive values at 45 ºC and 60 ºC, and, even turns to negative at 80 ºC.

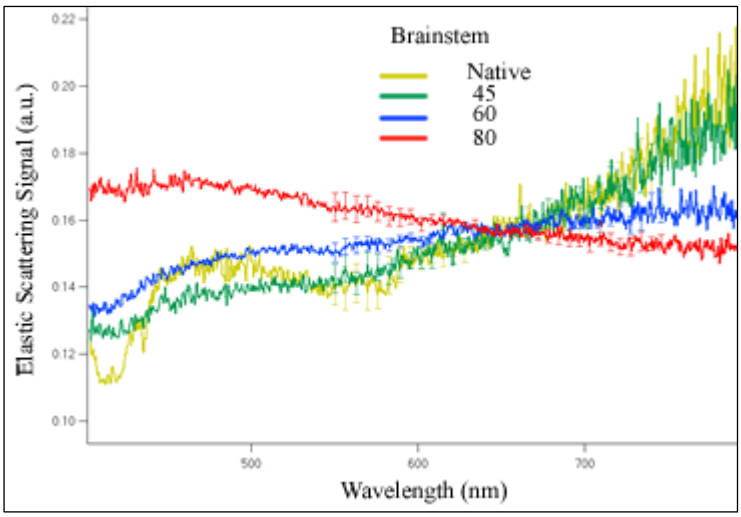

Figure 4.1. ESS spectra of lamb brain brainstem native, coagulated at 45 degrees Celsius, coagulated at 60 degrees Celsius, and coagulated at 80 degrees Celsius

When coagulated at different temperatures the slope of ESS spectra of cerebellum (Figure 4.2) shows a similar alteration to that of the brainstem data. While the slope of the ESS spectra of native cerebellum is 149.04 ± 1.41, the slope of the ESS spectra of cerebellum coagulated at 45 ºC is 22.368 ± 1.31, coagulated at 60 ºC is 17.236 ± 0.918, and coagulated at 80 ºC is -54.02 ± 0.677. As the coagulation temperature is increased the positive value of slope decreases and turns to negative.

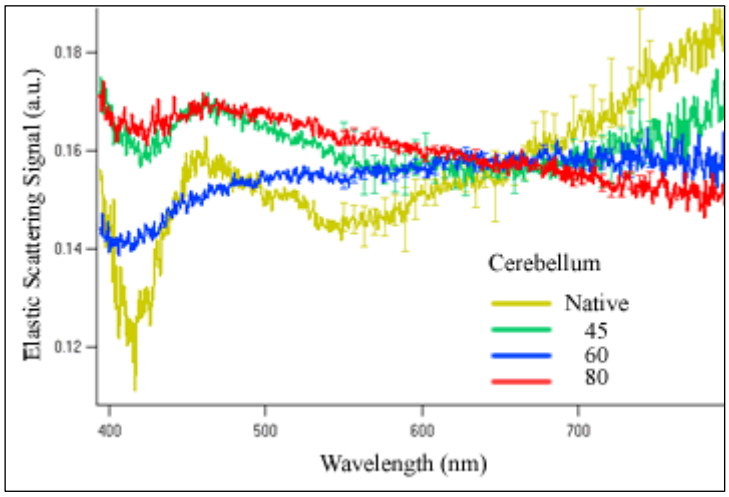

Figure 4.2. ESS spectra of lamb brain cerebellum native, coagulated at 45 degrees Celsius, coagulated at 60 degrees Celsius, and coagulated at 80 degrees Celsius

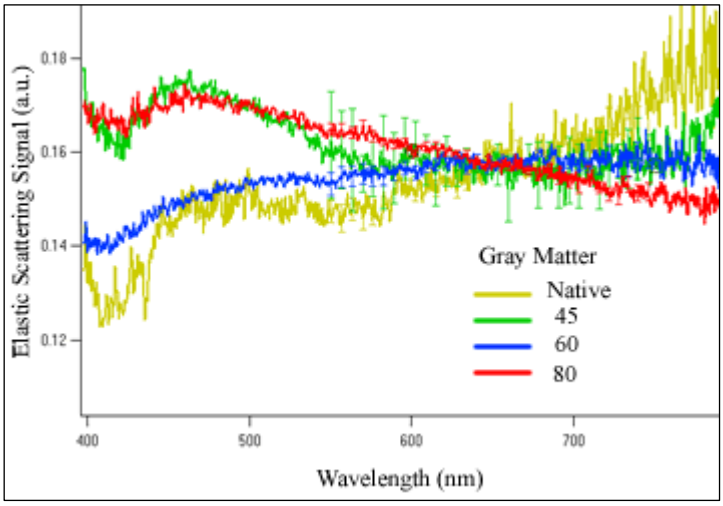

Figure 4.3. ESS spectra of lamb brain gray matter native, coagulated at 45 degrees Celsius, coagulated at 60 degrees Celsius, and coagulated at 80 degrees Celsius

The slope of the ESS spectra of native gray matter is 117.6 ± 2.12, the slope of the ESS spectra of gray matter coagulated at 45 ºC is -3.795 ± 1.58, at 60 ºC is 20.153 ± 0.87, and at 80 ºC is -71.76 ± 0.625. The slopes of the ESS spectra of native gray matter and gray matter that was coagulated at 60 ºC and 80 ºC are similar with cerebellum and brainstem. However the slope value for 45 ºC turns to negative if it is analyzed in visible wavelength range. There is an unexpected increase in the elastic scattering signal of gray matter that was coagulated at 45 ºC in the wavelength range of 450 nm 550 nm. If the graph is analyzed for the wavelength range of 600 nm to 750 nm the slope values are more

similar to brainstem and cerebellum but not the same (The slope of ESS spectra of native gray matter is 124.5 ±3.5, coagulated at 45 ºC is 5.59 ± 2.56, 60 ºC is 10.346 ± 1.35, and 80 ºC is -72.214 ± 0.99 in the wavelength range of 600 – 750 nm).

The slopes of ESS spectra of white matter are consistent with slope values for the ESS spectra of brainstem and cerebellum (The slope of the ESS spectra of native white matter is 218.71 ± 2.93, white matter coagulated at 45 ºC is 152.66 ± 2.29, at 60 ºC is 59.73 ± 0.88, and at 80 ºC is -74.503 ± 0.643). As the coagulation temperature is increased the slope of the ESS spectra decreases from the relatively high positive values of native white matter to lower positive values at 45 ºC and 60 ºC, and, even turns to negative at 80 ºC.

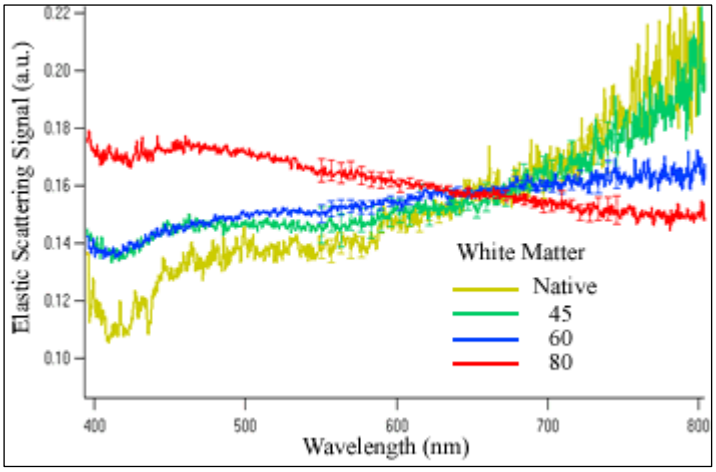

Figure 4.4 ESS spectra of lamb brain white matter native, coagulated at 45 degrees Celsius, coagulated at 60 degrees Celsius, and coagulated at 80 degrees Celsius

When the ESS spectra of native brain tissue parts from three different lamb brains are analyzed the correlated graphs can be taken. The graph of brainstem of first lamb brain is 97 % correlated with brainstem of second lamb brain in the visible wavelength range. The second is 90 % correlated with the third one and the first one is 93 % correlated with brainstem of third lamb brain (Figure 4.5).

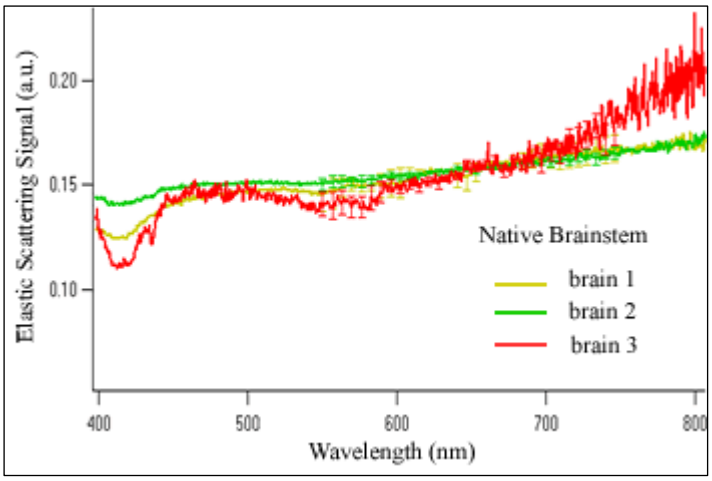

Figure 4.5 ESS spectra of native brainstem from three different lamb brain

The ESS spectrum of first lamb brain's native cerebellum is 65 % correlated with the ESS spectrum of second lamb brain cerebellum in the visible wavelength range. While the second is 50 % correlated with third one the first one is 83 % correlated with the ESS spectrum of third lamb brain cerebellum (Figure 4.6).

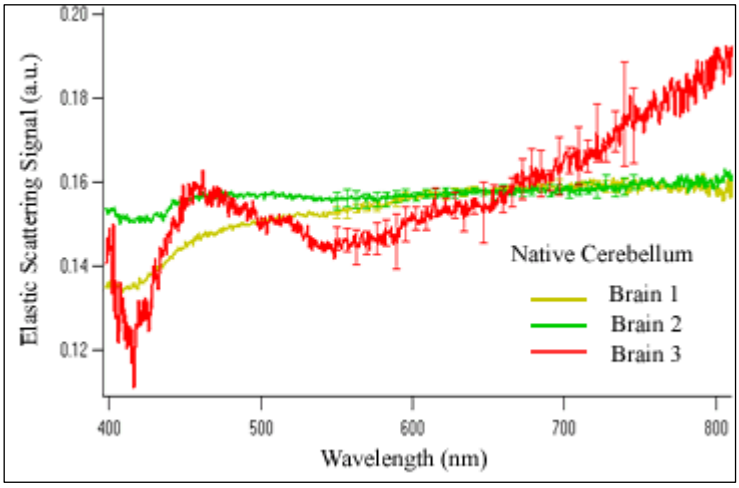

Figure 4.6 ESS spectra of native cerebellum from three different lamb brain

The ESS spectrum of first native gray matter is 93 % correlated with the ESS spectrum of second lamb brain gray matter. While the second is 79 % correlated with third one the first one is 91 % correlated with the ESS spectrum of gray matter of third lamb brain (Figure 4.7) in the visible wavelength range.

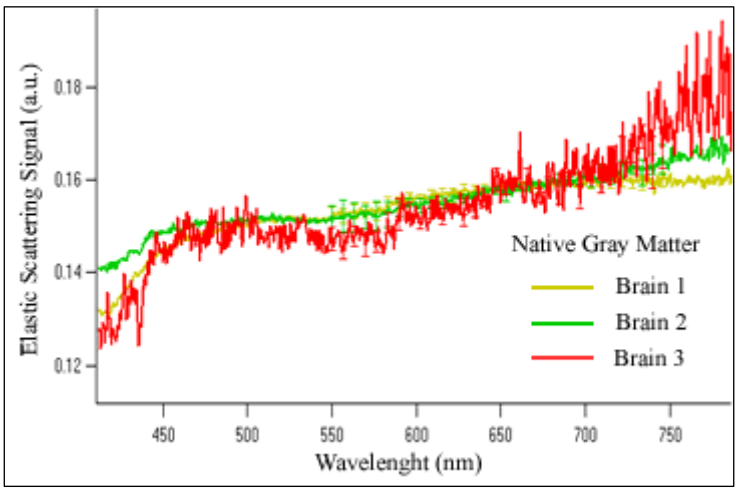

Figure 4.7 ESS spectra of native gray matter from three different lamb brain

The ESS spectrum of first native white matter is 99 % correlated with the ESS spectrum of cerebellum of second lamb brain in the visible wavelength range. While the second is 93 % correlated with third one the first one is 95 % correlated with the ESS spectrum of third lamb brain white matter (Figure 4.8).

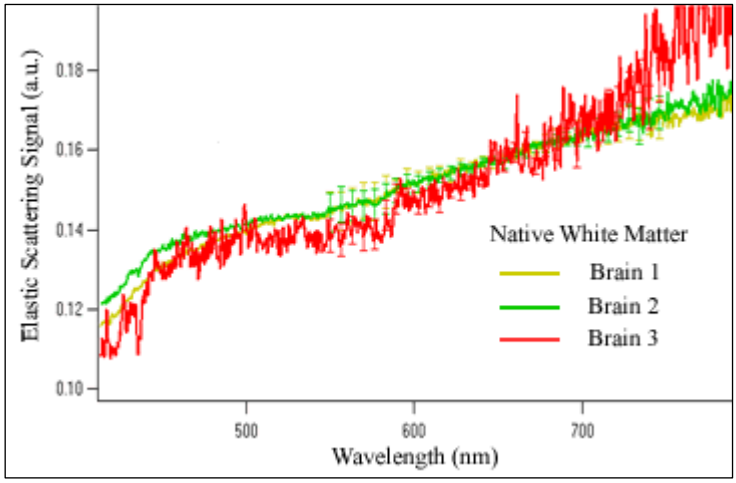

Figure 4.8 ESS spectra of native white matter from three different lamb brain

When the average of the elastic scattering signals of all native tissues from three lamb brains are graphed (Figure 4.9) it is observed that the average ESS spectra of the native brainstem, cerebellum, gray matter, and white matter are correlated to each other (the ESS spectra of native brainstem is 97 % correlated to cerebellum, gray matter, and white matter, the ESS spectra of cerebellum is 93 % correlated to gray matter, and it is 92 % correlated to white matter, the ESS spectra of gray matter is 98 % correlated to the ESS

spectra of native white matter). Although the spectra of these tissues are correlated they all have distinct patterns ($P < 0.005$). If the average elastic scattering signals of native tissues are analyzed according to the slopes they can be differentiated. Whole slopes are positive; however the slope values are different (the slope of average ESS spectra of native brainstem is 81.188 ± 1.01, cerebellum is 35.3 ± 0.63, gray matter is 53.38 ± 0.54, and white matter is 131.6 ± 0.75).

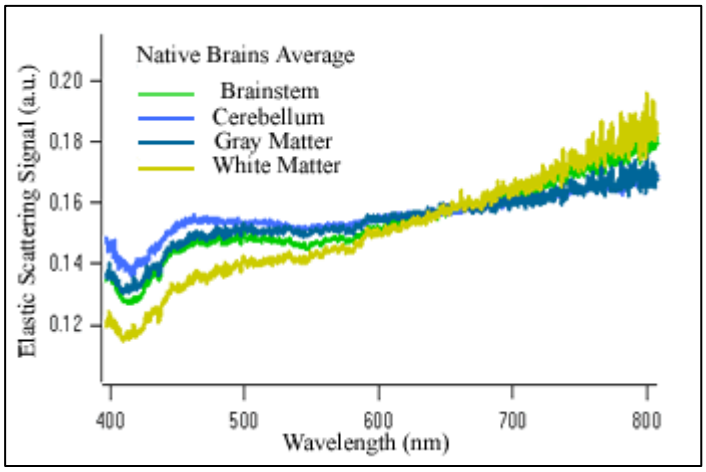

Figure 4.9 ESS spectra of average native brain tissues taken from three lamb brains

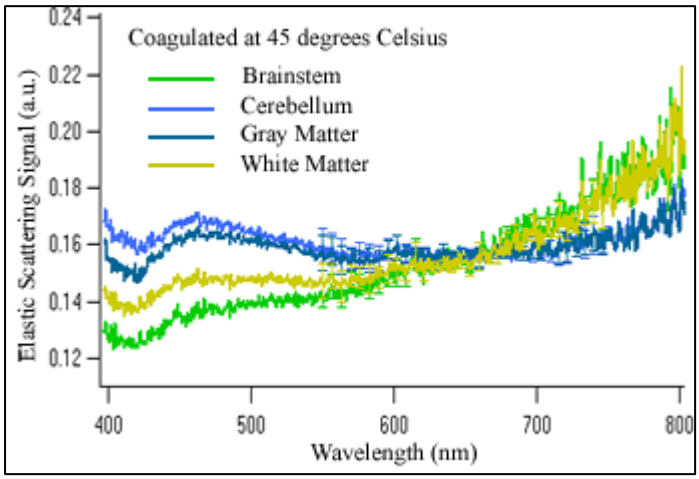

Figure 4.10 ESS spectra of lamb brain brainstem, cerebellum, gray matter, white matter coagulated at 45 degrees Celsius

When coagulated at 45 ºC (Figure 4.10) the ESS spectra of brainstem is % 96 correlated with white matter. There are no correlations between other tissues ($P < 0.001$). The slopes of the ESS spectra of these four tissues coagulated at 45 ºC are different from

each other (the slope of ESS spectra of brainstem coagulated at 45 ºC is 178.1 ± 2.44, cerebellum is 22.36 ± 1.31, gray matter is -3.79 ± 1.58, and white matter is 152.6 ± 2.29).

When brain tissues are coagulated at 60 ºC (Figure 4.11) the ESS spectra of brainstem is 96 % correlated with cerebellum 83 % with gray matter, and 88 % with white matter. The ESS spectra of cerebellum coagulated at 60 ºC is 93 % correlated with gray matter, and 95 % with white matter. There is 98 % correlation between gray and white matter. The difference between the slopes of the ESS spectra of brainstem and white matter coagulated at 60 ºC is not much (the slope of ESS spectra of brainstem coagulated at 60 ºC is 55.34 ± 0.94 and white matter is 59.73 ± 0.88). Also the difference between the slopes of cerebellum and gray matter spectra is not much (the slope of ESS spectra of cerebellum coagulated at 60 ºC is 17.23 ± 0.92 and gray matter is 10.34 ± 1.35).

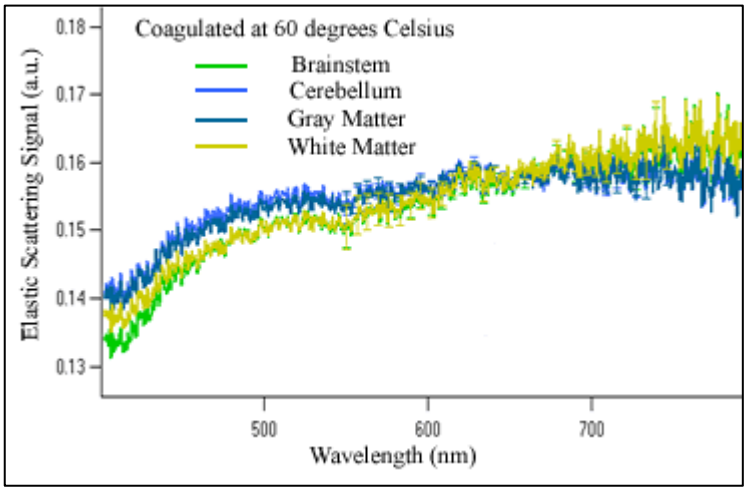

Figure 4.11 ESS spectra of lamb brain brainstem, cerebellum, gray matter, white matter coagulated at 60 degrees Celsius

The ESS spectra of four tissues that are coagulated at 80 ºC are 99 % correlated with each other (Figure 4.12). Spectra of all tissues have negative slope. There is very little difference between the slopes of the ESS spectra of brainstem, cerebellum, gray matter and white matter coagulated at 80 ºC (the slope of ESS spectra of brainstem coagulated at 80 ºC is -60.038 ± 0.67, cerebellum is -54.02 ± 0.67, gray matter is -71.67 ± 0.62, and white matter is -74.50 ± 0.64).

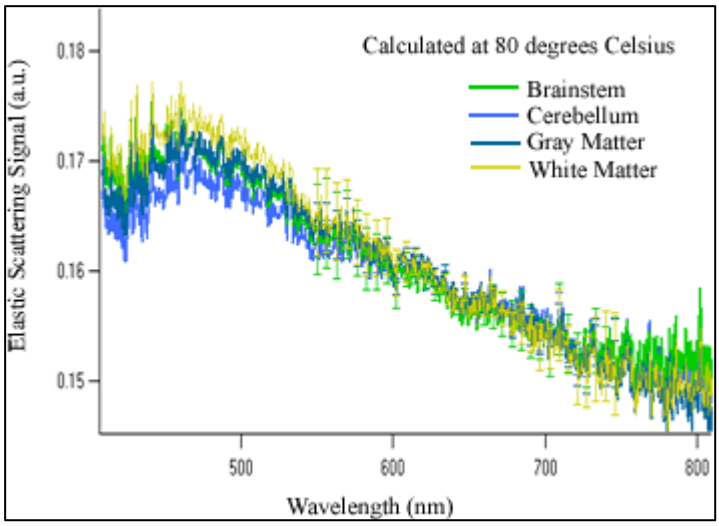

Figure 4.12 ESS spectra of lamb brain brainstem, cerebellum, gray matter, white matter coagulated at 80 degrees Celsius

4.3 Discussion

In this study, ESS spectra that were taken by CancerScanner system of four parts – brainstem, cerebellum, gray matter, white matter- of three lamb brains were analyzed. It was observed that as the coagulation temperature was increased; the slope of the ESS spectra decreased from the relatively high positive values of native brain tissues to lower positive values at 45 ºC (The only exception was gray matter coagulated at 45 ºC) and 60 ºC, and, even turned to negative values at 80 ºC.

At 45 ºC hyperthermia exists in tissue which means bond destruction and membrane alterations. At 60 ºC necrosis starts with the denaturation of proteins and collagens. Coagulation; the whitening of tissue is observed at 80 ºC. Coagulated tissue is composed of water-loss cells. In other words, nuclear to cytoplasmic ratio is changed. These changes on tissues which are coagulated at different temperatures can be detected. The morphological changes of cancerous tissues are nuclei enlargement and increased concentration of chromatin. It was observed that the slopes of ESS spectra taken with CancerScanner system in the visible range give information about alterations of nuclear to cytoplasmic ratio of tissues. Therefore analysis of slopes can be an appropriate method for tissue optics.

The ESS spectra of the brainstem, cerebellum, gray matter, white matter of three different native brain tissues have correlated graphs for each part. The analysis of native

brain tissues indicates that CancerScanner system gives similar spectra for same tissues. This shows the reliability of the system and the measuring method.

When analyzing the brain parts according to their being native or coagulated at different temperatures it was observed that for native brain the ESS spectra of brainstem, cerebellum, gray matter, and white matter have distinct pattern and brain parts can be differentiated according to the slopes of their ESS spectra. After increasing the coagulation temperature especially over hyperthermia the graphs of tissues are more similar to each other and the slopes are getting closer.

5. *IN SITU* MEASUREMENTS

In this study, CancerScanner system was firstly examined on human biopsy tissues. The measurements were done in the Operating-Room of Istanbul University, Istanbul Faculty of Medicine and Institute of Neurological Sciences Pathology Laboratory, Marmara University, Istanbul, Turkey. The results were compared at the same time with that of pathologic examination of the appropriate tissues under the control of pathologists. Since the *in situ* experiment results on animals with this system [15] indicated that the ESS spectra of normal tissues have positive slope and of cancerous tissues have negative slope it is expected that the ESS spectra would have negative slope for cancerous, and positive slope for normal human biopsy tissues in visible wavelengths.

This is the first use of CancerScanner system in clinics to diagnose cancer on human biopsy tissues. ESS spectra were examined to find if this system may differentiate cancerous tissues from normal tissues.

5.1 Methods

In this study measurements were taken by touching the tip of the probe to different human tissues and monitoring the elastic scattering signal from the interface on PC screen after CancerScanner system was calibrated (this procedure was described in detail in chapter 3).

All measurements were taken from *in situ* biopsy particle during surgery just after the human tissue was dissected by the surgeon. There were no other process between the measurement and surgery. The biopsy samples were brought to the pathology room from the operating room by the surgeon while the patient is anesthetized. Tissues were not stained or fixed. The histopathologist examined the tissues after elastic scatter spectra were taken. Approximately 7-15 measurements were taken from each sample. The averages of the spectra were calculated between 550-750 nm wavelengths for each different sample.

When analyzing the spectra of normal and abnormal tissues, the slope of the elastic scatter signal curve was used in the visible wavelength range. The slopes were normalized ($x10^6$). Student *t*-test and correlation were used for statistical analysis.

5.2 Results

5.2.1 Lung Tissue and Paratracheal Lymph Node

There were 7 patients and 15 lung or paratracheal lymph node tissues -3 of which were normal and the rest were tumors- were dissected and analyzed comparatively by CancerScanner system and histopathologic methods.

The ESS spectra of 70 years old male patient's normal and cancerous lung tissue is seen in Figure 5.1. This patient has a medullar and follicular thyroid cancerous tumor. There is metastasis in the right inferior lobe of the patient's lung. The ESS spectra of the tumor's black regions that were result of smoking and air pollution and the tumor surface are 99% correlated and have negative slopes (Black regions: -79.05 ± 0.658 and tumor surface: -95.399 ± 0.842). Non-cancerous parts of the dissected right inferior lobe gave positive slope (+70.173 ± 1.59) of elastic scattering signal in the interval of 600-750 nm as expected. The ESS of normal and tumor are significantly different ($P < 0{,}001$).

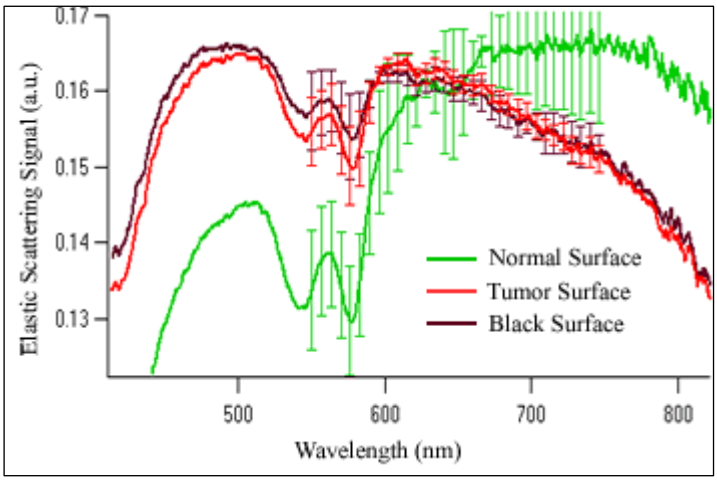

Figure 5.1 The ESS spectra of tumor that is the metastasis of medullar and follicular thyroid cancer in the right inferior lobe of the 70 years old male patient's lung

The same patient's paratracheal lymph node was examined to see if there was cancer methastasis to the node. Methastasis was diagnosed histopathologically in the paratracheal

lymph node of the patient. ESS spectra had negative slope (-77.361 ± 0.641) in 600-750 nm wavelength interval (Figure 5.2), this result overlaped with that of histopathology report. The black regions in that paratracheal lymph node has also a correlated spectrum (99%) with the tumor. It's slope is negative (-44.351 ± 1.42).

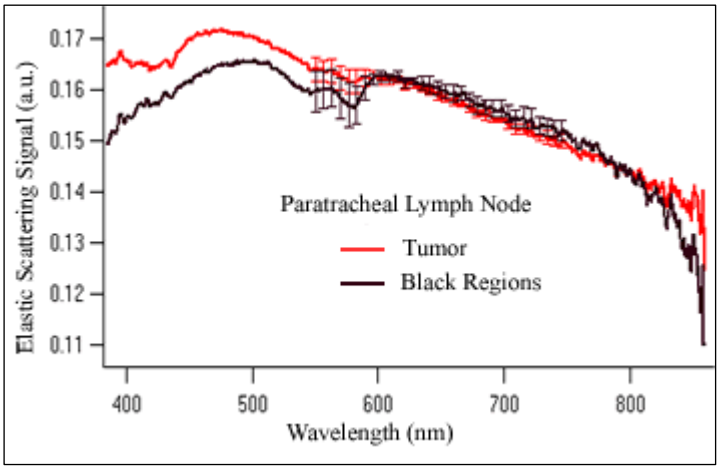

Figure 5.2 70 years old male patient's cancerous paratracheal lymph node that is the methastasis of medular and follicular thyroid cancer

The ESS spectrum of tumor from right inferior lobe of lung of 59 years old male is seen in Figure 5.3. The clinical diagnosis of the tumor was pleomorphic carcinoma. The results taken from ESS spectra and histopathology were both compatible with clinical reports. ESS spectra of tumor and the surface of this tumor have negative slopes (tumor: -120.66 ± 1.24, surface of the tumor: -18.95 ± 1.4). The ESS spectrum of normal tissue has positive slope (22.43 ± 1.21). Normal and tumor tissue spectrum is significantly different ($P < 0.001$).

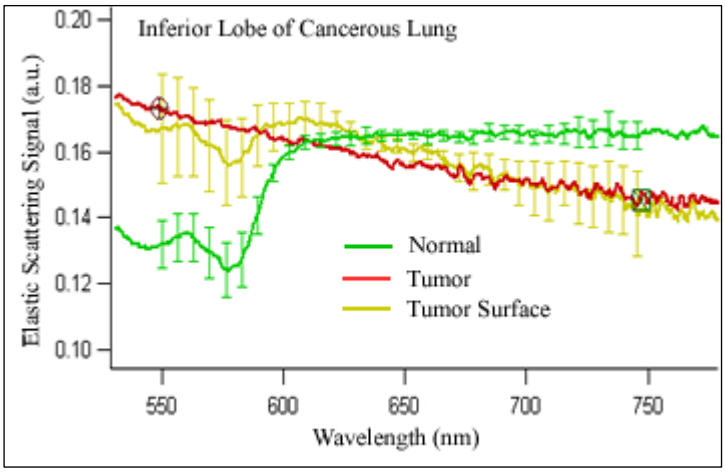

Figure 5.3 Elastic scattering spectra of cancerous lung tissue of 59 years old male

System detected the cancerous parts surrounding of a tumor. 63 years old male patient's superior lobe of the right lung was dissected. Elastic scatter signal of both tumor and its surrounding tissue has negative slope (tumor: -2.753 ± 0.454 surrounding tissue: -21.514 ± 0.23) (Figure 5.4). Tumor spectrum and the surrounding is 79% correlated. According to histopathology report the lobectomy sample was necrotic and there were fibrosis, hyalinization, inflammatory infiltration, and malignant tumor cells in the surrounding. The appearance of malignant tumor cells in this report is compatible with ESS results.

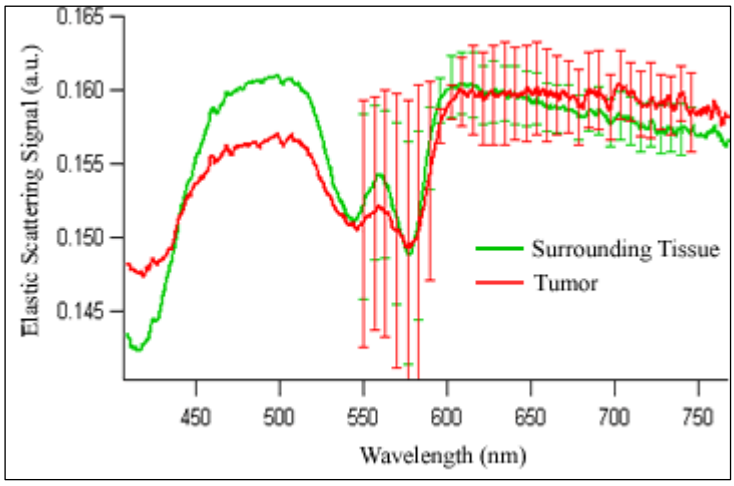

Figure 5.4 Elastic scatter spectrum of malignant tumor and it's surrounding in the superior lobe of the right lung of 63 years old male patient

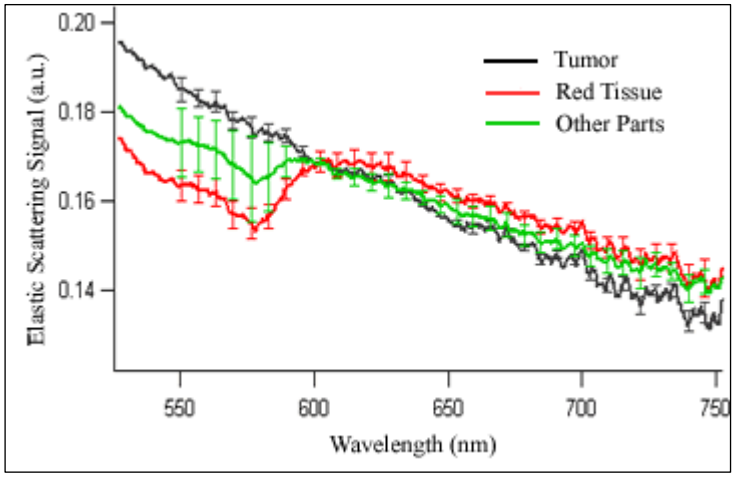

Figure 5.5 Elastic scatter spectrum of an adeno carsinoma tumor of lung tissue in the left inferior lobe from 78 years old male

In Figure 5.5 the ESS spectra of three different parts of the cancerous lung tissue of 78 years old male are seen. These tissues' average ESS spectra are 99% correlated.

Histopathologically, this tumor was adeno carsinoma and there were malignant cells in all these three tissue samples (the first part of tumor slope is -244.99 ± 1.49, the second part of tumor slope is -195.82 ± 1.24, and the surrounding tissue slope is -189.72 ± 0.851).

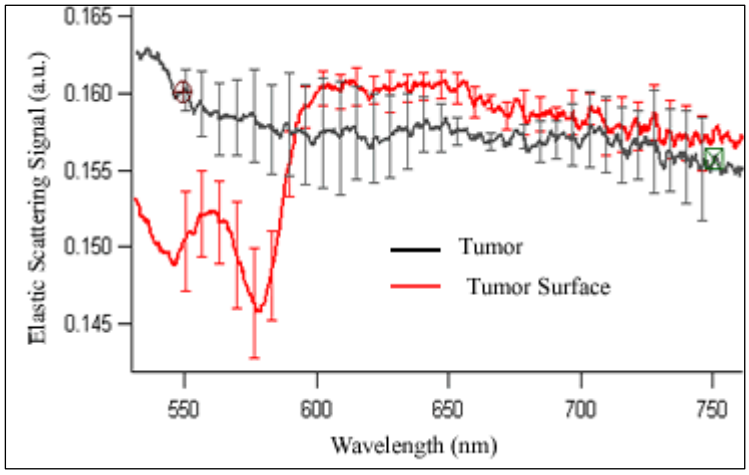

Figure 5.6 Elastic scattering spectra of adeno carsinoma lung tissue of 78 years old male

ESS spectrum that is seen in Figure 5.6 was taken from lung tissue (male, 78 years old) which is diagnosed as adeno carsinoma. Tumor and its surface is 82 % correlated. Slope of tumor graph is -11.456 ± 0.54, and the slope of surface is -27.518 ± 0.492. They are negative as expected for cancerous lesions.

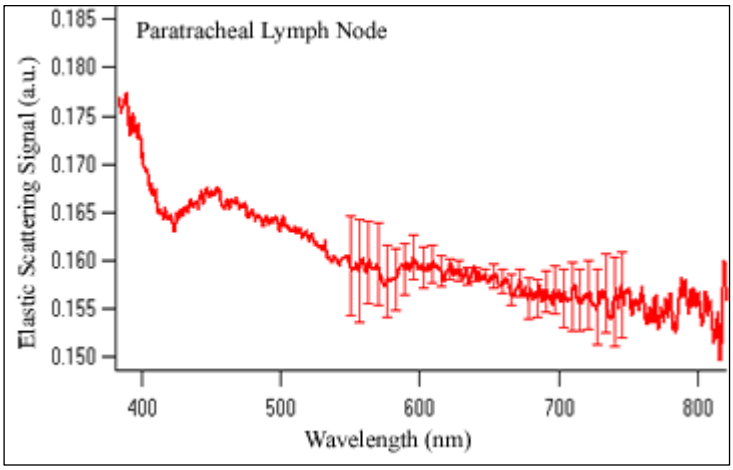

Figure 5.7 The elastic scatter signal graph of the pre-trachea lymph node from a 53 years old female who is thyroid cancer

The ESS spectrum of lymph node that was taken from a 53 years old female is seen in Figure 5.7. This patient was taken to surgery with thyroid cancer diagnosis and there was a doubt about cancer metastasis to the lymph nodes. According to the histopathology

report there was no tumor in that paratracheal lymph node, only reactive changes occurred. Elastic scatter spectra gave a negative slope (-14.788 ± 0.675) between 600 and 750 nm wavelengths.

Another unexpected graph is seen in Figure 5.8. This 70 years old male patient has a lung tumor in left inferior lobe. In first examination during surgery there were two possibilities according to histopathologist: 1) atypical adenomatous hyperplasia and 2) broncialveolar lung tumor. After another more detailed examination by histopathologists it was diagnosed as an atypical adenomatous hyperplasia which is not cancerous tissue type. The result was misleading and the ESS spectrum had negative slope like in cancerous lesions.

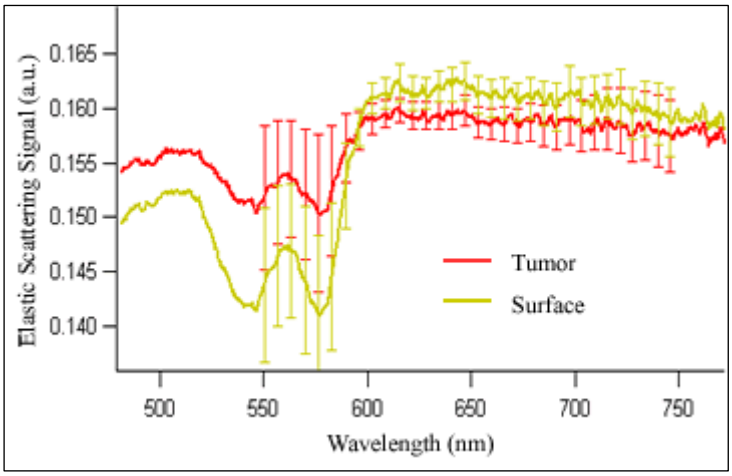

Figure 5.8 The ESS spectra of lung tumor in left inferior lobe of 70 years old male patient

This graph (Figure 5.8) also shows that both tumor and its surface have negative slopes: -10.65 ± 0.398 and -15.119 ± 0.594 respectively. There is 99 % correlation between surface and tumor spectra in the visible range.

As it is seen from all the spectra interval of 550-600 nm the standard deviations are high due to the blood absorption band in that space. Lung is very bloody and if the analysis includes that interval it would give misinformation about the slopes. This is why the measurements in between 600-750 nm were analyzed.

In this study, the efficiency of CancerScanner system was reported in Table 5.1 comparatively with the results of histhopathological examinations. Measurements from 15 lung and paratracheal lymph node tissues of 7 patients showed that, CancerScanner system

results was inconsistent with histopathologic report for only 2 tissues (Table 5.1, no 14, 15). It can be reported that the predictive value of the CancerScanner system is 86.6 % for lung tissues and paratracheal lymph nodes in differentiating cancerous and normal tissues. The ESS spectra of all cancerous tissues have negative slopes as expected. Therefore the sensitivity of the system is 100 %. It gave positive slope for two of the three normal tissues. The specificity of CancerScanner system is 66.6 % for lung and paratracheal lymph nodes. The tissue (Table 5.1, no 14) whose ESS spectrum has negative slope shows reactive alterations according to histopathology report.

The ESS spectrum of abnormal but non-cancerous tissue has negative slope (Table 5.1, no 15). This study on lung and paratracheal lymph node does not give statistically meaningfull data in differentiating cancerous tissue from abnormal tissues.

Table 5.1
Tissues, Pathologic Diagnosis, and CancerScanner System Success for Lung and Paratracheal Lymph Nodes

No	Category	Pathology Report	ESS	Success
1	Cancer	Lung, Medullar & Follicular Thyroid Cancer	Negative Slope	√
2	Cancer	Lung Medullar & Follicular Thyroid C. /Black Regions	Negative Slope	√
3	Normal	Lung	Positive Slope	√
4	Cancer	Paratracheal Lymph Node, Thyroid C. Metastasis	Negative Slope	√
5	Cancer	Paratracheal Lymph N. Thyroid C. Metastasis /Black R.	Negative Slope	√
6	Cancer	Lung, Pleomorphic Carcinoma	Negative Slope	√
7	Normal	Lung	Positive Slope	√
8	Cancer	Lung, Carsinoma	Negative Slope	√
9	Cancer	Lung, Carsinoma	Negative Slope	√
10	Cancer	Lung, Adeno Carsinoma	Negative Slope	√
11	Cancer	Lung, Adeno Carsinoma	Negative Slope	√
12	Cancer	Lung, Adeno Carsinoma	Negative Slope	√
13	Cancer	Lung, Adeno Carsinoma	Negative Slope	√
14	Normal	Paratracheal Lymph Node, Reactive Changes	Negative Slope	X
15	Tumor	Lung, Atypical Adenomatous Hyperplasia	Negative Slope	X

5.2.2. Brain Tissue

There were 7 patients and 10 brain tissues -8 of which were tumors and only 2 of them were normal- were dissected and analyzed by CancerScanner system and histopathologic methods (Figure 5.9).

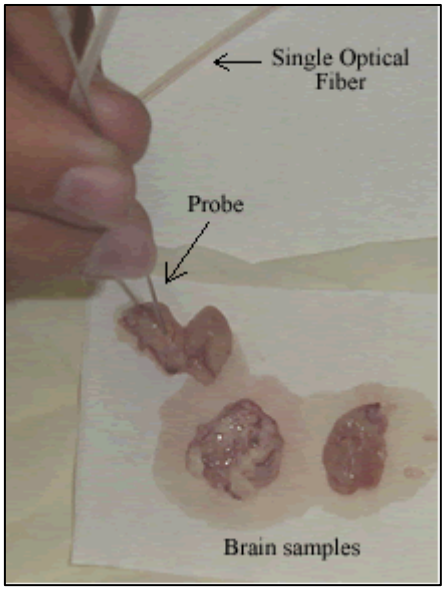

Figure 5.9 The picture of brain tissues taken during experiment

Elastic scattering spectrum of 36 years old male patient's brain tumor is seen in Figure 5.10. This tumor was diagnosed as chordoma after pathological examination. Spectrum has negative slope (-54.39 ± 0.408) in visible wavelength range, as expected for cancerous tissues.

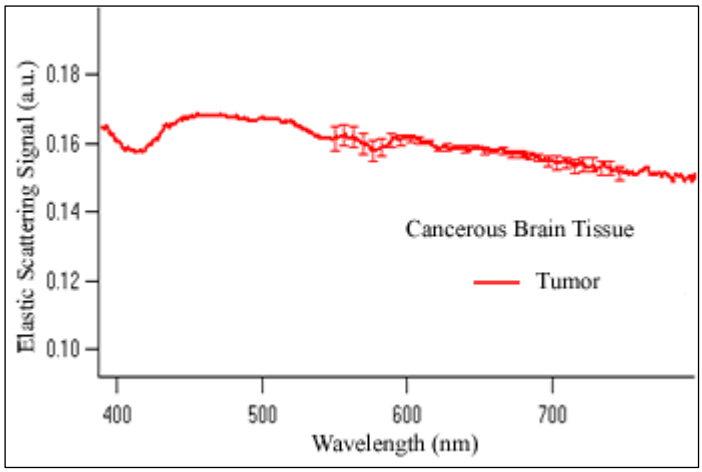

Figure 5.10 ESS spectra of 36 years old male patient's brain tumor

72 years old male patient has neuroepithelial brain tumor that was diagnosed as glioblastoma by histopathology. The elastic scattering spectrum of normal brain tissue of this patient has positive slope (29.6 ± 0.407) and cancerous tissue has negative slope

(-31.97 ± 0.465) in the visible range (Figure 5.11). These results are consistent with the expected ones.

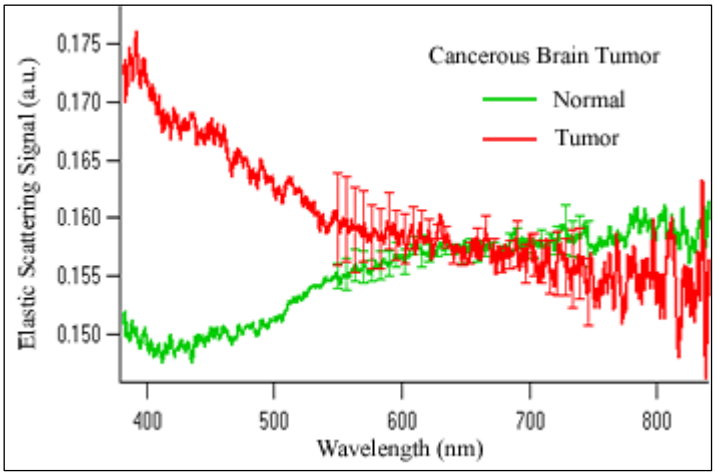

Figure 5.11 ESS spectra of 72 years old male patient's brain tumor

The brain tumor of 57 years old female patient was dissected in surgery. This tumor was diagnosed as an atypical meningioma by histopathologist. Meningioma is a kind of benign tumors. The elastic scattering spectrum of the tumor has negative slope (-112.97 ± 0.601) (Figure 5.12).

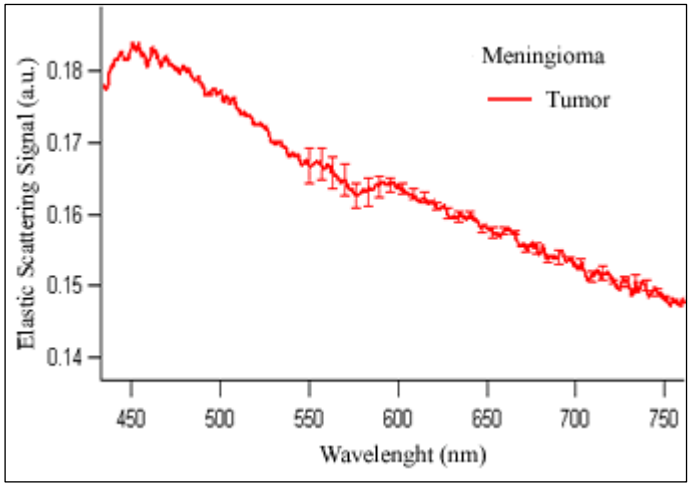

Figure 5.12 ESS spectra of 57 years old female patient's benign tumor

Figure 5.13 shows the ESS spectra of brain tumor of 70 years old male patient. This tumor is glioblastoma that infiltrated to normal tissue. System could not differentiate the normal tissue from cancerous this might be due to the infiltration. ESS

spectra have positive slopes for two parts (normal tissue: 64.374 ± 0.393, infiltration: 57.928 ± 0.424).

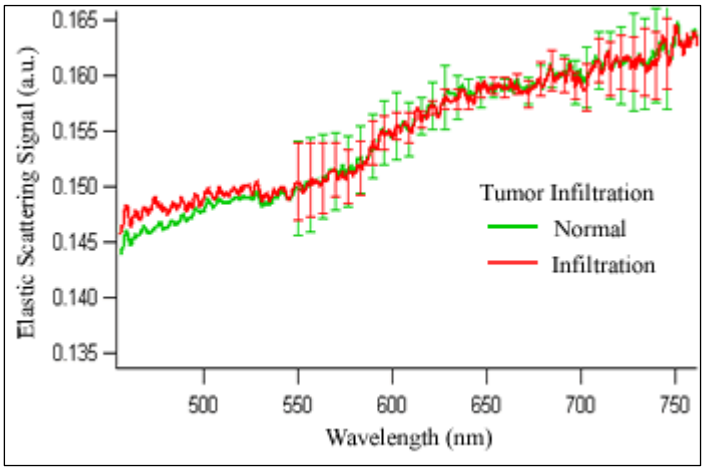

Figure 5.13 ESS spectra of 70 years old male patient's brain tumor

A tumor in third ventricle of 47 years old female patient was dissected. It was diagnosed as colloid cysts by histopathology. The ESS spectrum (Figure 5.14) of cysts has negative slope (-25.3 ± 0.248).

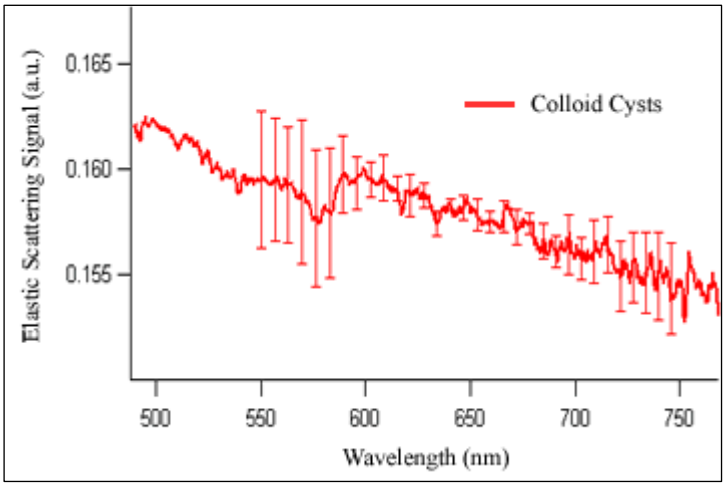

Figure 5.14 ESS spectra of 47 years old female patient's colloid cysts

In Figure 5.15 the ESS spectra of brain tumor taken from 30 years old female patient is seen. While the clinical diagnosis was Schwannom, histopathological diagnosis was meningioma. Negative slope was expected for tumors but the slope of ESS spectrum has positive slope (8.12 ± 0.336).

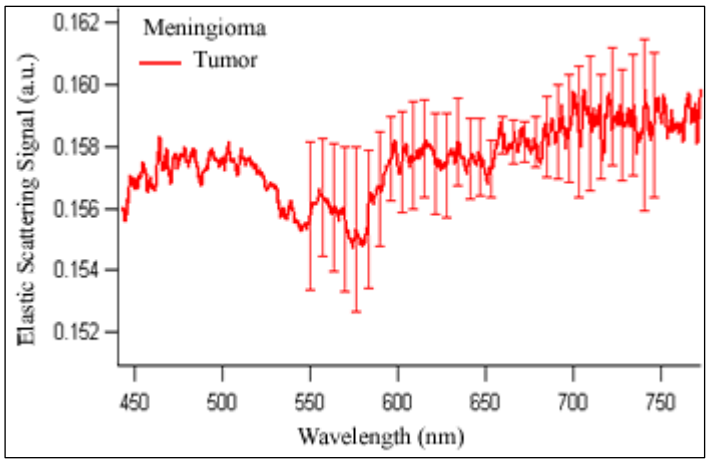

Figure 5.15 ESS spectra of 30 years old female patient's brain tumor

28 years old female patient brain tumor was dissected and two different types of abnormal tissues were analyzed by CancerScanner system and histopathology. First one was papilloma and other was abnormal soft tissue that includes cancerous cells. The ESS spectra of both tissues had negative slope as expected (Figure 5.16). The slope of papilloma was -88.97 ± 0.702 and the slope of other tissue was -113.03 ± 0.59.

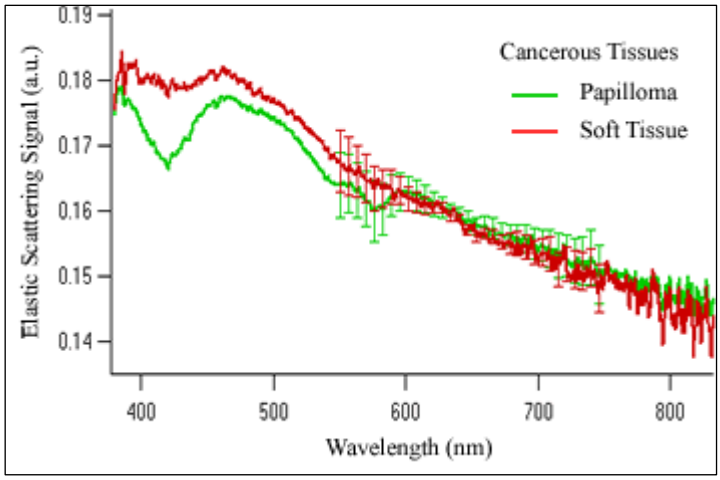

Figure 5.16 ESS spectra of 28 years old female patient's brain tumor

In this study, CancerScanner system gave two inconsistent results with histopathology out of ten samples (Table 5.2). It can be reported that the success rate of the CancerScanner system is 80 % in differentiating tumor from normal tissue for brain tissues. The sensitivity and specificity of the system is 75 % and 100 % respectively in detecting brain tumors.

The ESS spectra of tumors (non-malignant tissues) have negative slopes (Table 5.2). This study on brain tissue does not give statistically meaningfull data about differentiating cancerous tissue from benign tumors.

Table 5.2

Tissues, Pathologic Diagnosis, and CancerScanner System Success for Human Brain Tissue

Sample	Category	Pathology Report	ESS	Success
1	Cancer	Chordoma	Negative Slope	√
2	Cancer	Glioblastoma	Negative Slope	√
3	Normal	Brain	Positive Slope	√
4	Benign Tumor	Meningioma	Negative Slope	√
5	Cancer	Glioblastoma	Positive Slope	X
6	Normal	Brain	Positive Slope	√
7	Tumor	Colloid Cysts	Negative Slope	√
8	Cancer	Glioblastoma	Positive Slope	X
9	Tumor	Papilloma	Negative Slope	√
10	Tumor	Cancerous Soft Tissue	Negative Slope	√

5.2.3. Breast Tissue

18 breast tissues from 7 patients -5 of them were tumors and others were fatty and normal tissues- were dissected and analyzed histopathologically and with CancerScanner system.

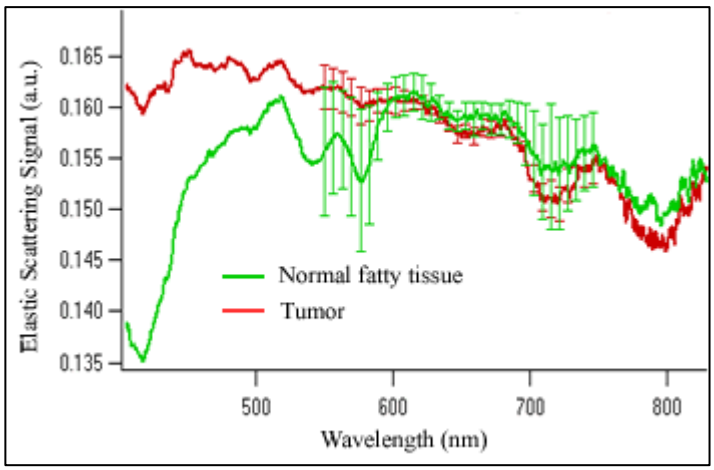

Figure 5.17 ESS spectra of 37 years old female patient's breast tumor

37 years old patient's breast was dissected and analyzed histopathologically and it was diagnosed as invasive ductal carsinoma. The ESS spectrum of tumor has expected negative slope (-43.16 ± 0.528) in the visible range for cancerous tissues (Figure 5.17). For healthy or normal tissues positive slope is expected but the ESS spectrum of normal fatty tissue has negative slope (-48.31 ± 0.915).

The ESS spectra of different parts of 59 years old female patient's normal breast tissue are seen in Figure 5.18. It is not cancerous according to histopathology report. This fatty tissue has fibrosis and inflammation. While the slope of ESS spectrum of one of these different parts is positive others are negative (the slope of ESS spectrum of yellow tissue is 49.57 ± 0.601, white tissue is -10.84 ± 0.28, and other tissue is -4.83 ± 0.36). It was expected to have all these slopes to be positive.

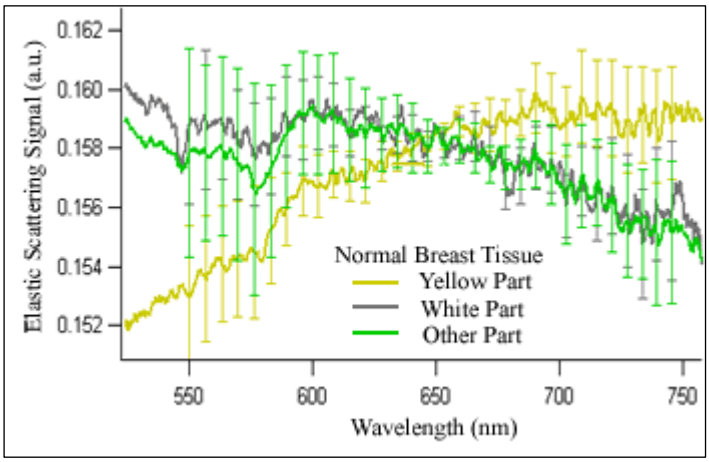

Figure 5.18 ESS spectra of 59 years old female patient's different parts of breast tissue

44 years old female patient's cancerous breast tumor was dissected and after histopathological examination it was reported to be as carsinoma. The slopes of ESS spectra are not consistent for cancerous parts (Figure 5.19). The slopes of tumor and dysplasia (that was mentioned in chapter 2) are positive (22.34 ± 0.46) but it was expected to be negative. The ESS spectrum of normal muscle tissue which was dissected from the bottom of breast has positive slope (110.85 ± 0.464) in the visible range as expected.

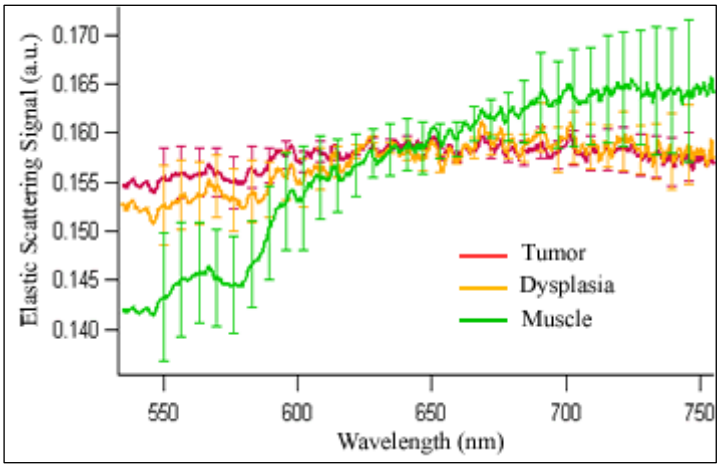

Figure 5.19 ESS spectra of 44 years old female patient's different parts of breast tissue

The ESS spectra of different parts of 44 years old female patient's breast tissue are seen in Figure 5.20. These tissues have reactive alterations and abscess according to histopathology report. Although there is no cancerous lesion the ESS spectra have negative slopes for all three different tissues (the slope of the ESS spectrum of fat tissue is -89.871 ± 0.317, red tissue is -122.58 ± 0.692, and fatty normal tissue is -161.16 ± 0.274).

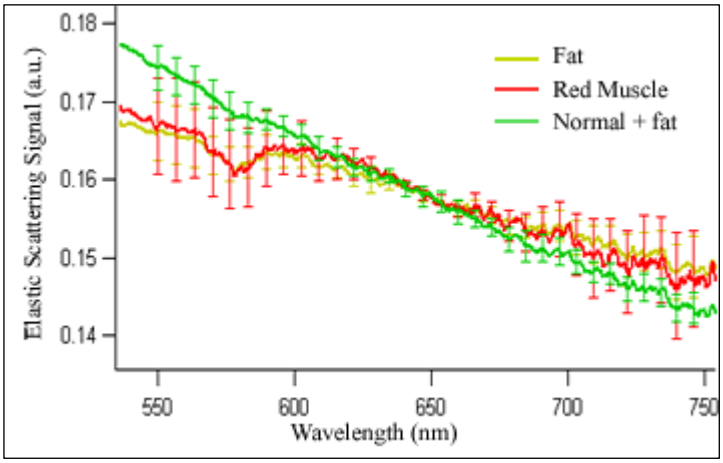

Figure 5.20 ESS spectra of 44 years old female patient's different parts of breast tissue

64 years old patient's dissected breast tissue was diagnosed as invasive ductal carsinoma by histopathology. When it was analyzed with CancerScanner system it was observed that the ESS spectrum of tumor had negative slope (-98.79 ± 0.35) as expected and the non-cancerous but fatty tissue had negative slope (-241.17 ± 2.02) (Figure 5.21). Tumor graph is consistent with expected.

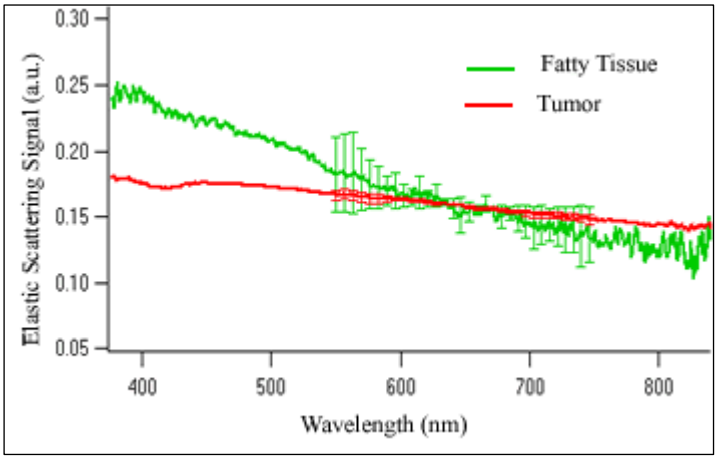

Figure 5.21 ESS spectra of 64 years old female patient's breast tissue

Breast tissue was diagnosed as intraductal papilloma by histopathology. When it was analyzed with CancerScanner system it was observed that the ESS spectrum of tumor had positive slope (9.1046 ± 0.458) and it is not consistent with the expected (Figure 5.22). The normal breast tissue has positive slope (47.631 ± 0.318) so this is consistent. The ESS spectra of fatty tissue has negative slope (-24.077 ± 0.554).

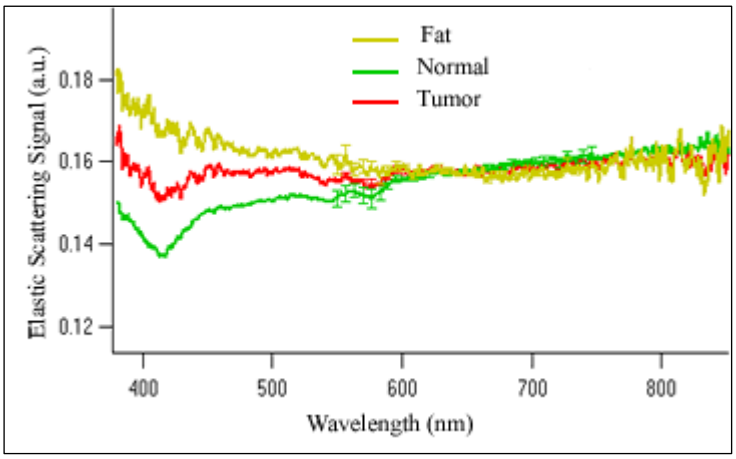

Figure 5.22 ESS spectra of female patient's breast tissue

39 years old female patient's cancerous breast tumor was dissected. It was diagnosed as carsinoma in red muscles histopathologically. The slopes of ESS spectra were taken from non-cancerous parts of the breast (Figure 5.23). The slope of ESS spectrum of fatty normal tissue was 12.247 ± 0.627, the pectoral muscle was -15.414 ± 0.819 in the visible range. While spectrum of normal tissue is consistent with the expected one the spectrum of pectoral muscle is not consistent. It should have negative slope.

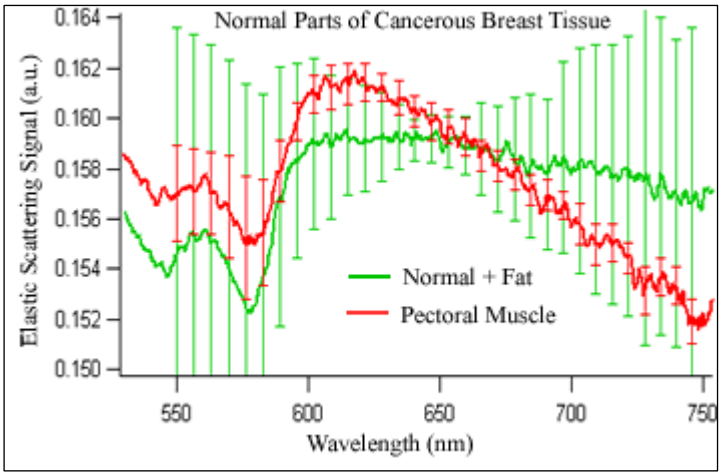

Figure 5.23 ESS spectra of 39 years old female patient's normal parts of cancerous breast

Table 5.3

Tissues, Pathologic Diagnosis, and CancerScanner System Success for Human Breast Tissue

Sample	Category	Pathology Report	ESS	Success
1	Tumor	Invasive Ductal Carsinoma	Negative Slope	√
2	Normal	Fatty Breast Tissue	Negative Slope	X
3	Normal	Breast	Positive Slope	√
4	Normal	Breast	Negative Slope	X
5	Normal	Breast	Negative Slope	X
6	Tumor	Carsinoma	Positive Slope	X
7	Tumor	Dysplasia	Positive Slope	X
8	Normal	Muscle Tissue	Positive Slope	√
9	Normal	Fat	Negative Slope	X
10	Normal	Red Muscle Tissue	Negative Slope	X
11	Normal	Fatty Breast Tissue	Negative Slope	X
12	Tumor	Invasive Ductal Carsinoma	Negative Slope	√
13	Normal	Fatty Breast Tissue	Negative Slope	X
14	Normal	Breast	Positive Slope	√
15	Tumor	Intraductal Papilloma	Positive Slope	X
16	Normal	Fatty Breast Tissue	Negative Slope	X
17	Normal	Fatty Breast Tissue	Positive Slope	√
18	Normal	Muscle Tissue	Negative Slope	X

Results of measurements on breast tissues are not as expected this can be due to the fat. The diagnoses of 4 of 13 normal tissues were consistent with histopathology report (Table 5.3). Only 2 of the 5 tumor could be differentiated. The sensitivity and the specificity of the CancerScanner system are 40 % and 30.77 % respectively in differentiating tumor from normal for breast tissue. The predictive value of the system in breast cancer diagnosis is 33.33 %.

System could not differentiate fat from tumor (P>0.001). 5 of the 6 fat or fatty tissues had negative slopes like cancerous lesions. These experiments on breast tissue showed that the fatty tissues give negative slopes.

5.2.4. Other Tissues

A nodule in thyroid of 53 years old female patient was examined. This nodule was diagnosed as carsinoma by histopathology. The ESS spectra of this nodule and its surrounding tissue have negative slopes (nodule: -120.24 ± 1.48, surrounding tissue: -59.218 ± 5.28) in the visible range (Figure 5.24). The slope of ESS spectrum of nodule is consistent with the diagnosis of pathology however, the ESS spectrum of surrounding tissue is not since there were no cancerous cells surrounding of the nodule according to

histopathology. These two different tissues are significantly different from each other ($P < 0.001$) but they are 91 % correlated.

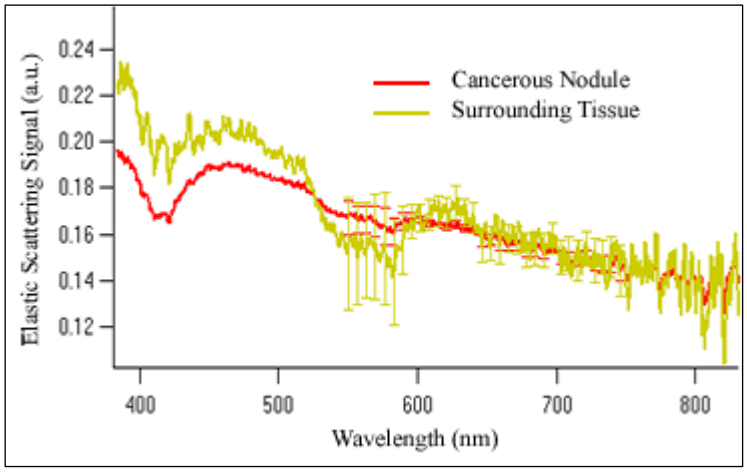

Figure 5.24 ESS spectra of 53 years old female patient's cancerous nodule

Thyroid of 42 years old female patient was dissected and diagnosed as nodular colloidal goitre. The ESS spectra of both normal and nodule tissue have negative slopes (nodule: -226.9 ± 0.95, normal tissue: -110.1 ± 2.26) that was not consistent with the expected (Figure 5.25).

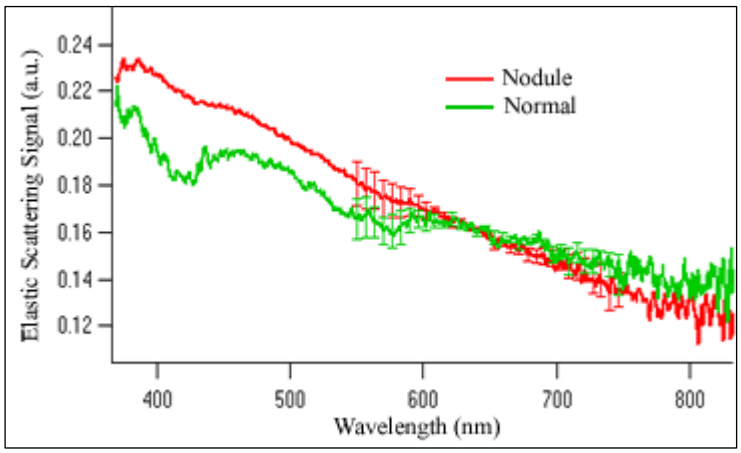

Figure 5.25 ESS spectra of 42 years old female patient's nodule and normal thyroid tissue

The thyroid of 48 years old female patient was dissected since there was a nodule in it. This nodule was not a cancerous according to histopathology. The ESS spectra of both normal thyroid tissue and nodule have negative slope (normal tissue: -16.537 ± 1.02, nodule: -54.47 ± 0.621) in the wavelength range of 600 - 750 nm (Figure 5.26). This is not compatible with the histopathology report.

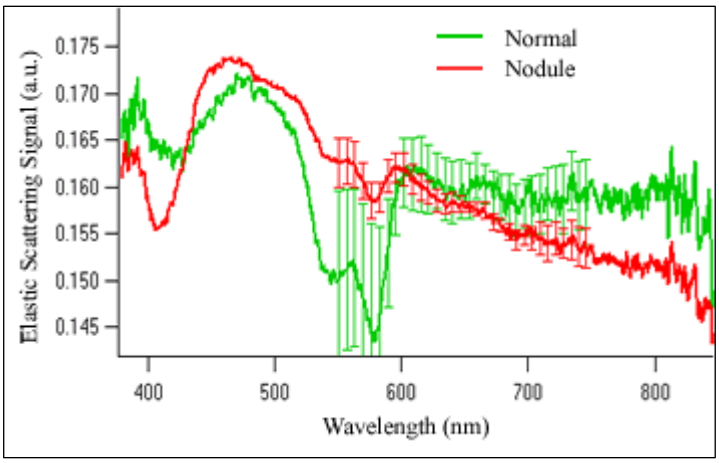

Figure 5.26 ESS spectra of 48 years old female patient's nodule and normal thyroid tissue

The thyroid of 37 years old male patient was dissected and diagnosed as nodular goitre. The ESS spectra of the nodule and normal thyroid tissue have both negative slopes (nodule: -40.5 ± 0.342, normal: -55.67 ± 0.807) (Figure 5.27). CancerScanner system could not differentiate normal tissue and nodule.

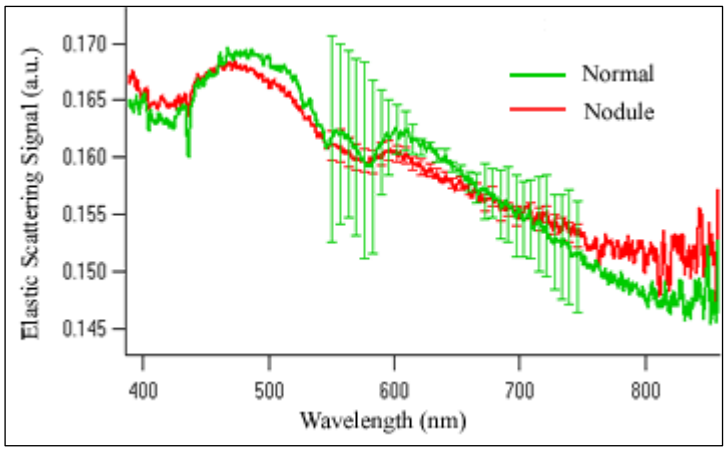

Figure 5.27 ESS spectra of 37 years old male patient's nodule and normal thyroid tissue

The thyroid of 32 years old female patient was diagnosed as hyperplasia by histopathologist. The ESS spectra of tissue have negative slope (-64.46 ± 0.855) (Figure 5.28). This result is consistent with the histopathology report.

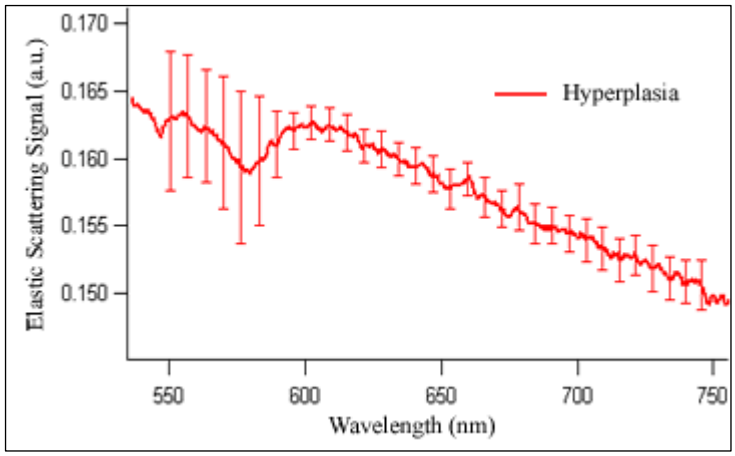

Figure 5.28 ESS spectra of 32 years old female patient's hyperplastic thyroid tissue

A gall bladder tissue taken from a 62 years old male patient examined histopathologically and by CancerScanner system. A suspicious tissue was not diagnosed as cancer, it was chronic colecystit. The ESS spectrum of this suspicious tissue had negative slope (-60.8 ±0.52) as expected for cancerous lesions (Figure 5.29). The slope of ESS spectrum of ulcer was positive (110.51 ± 0.3).

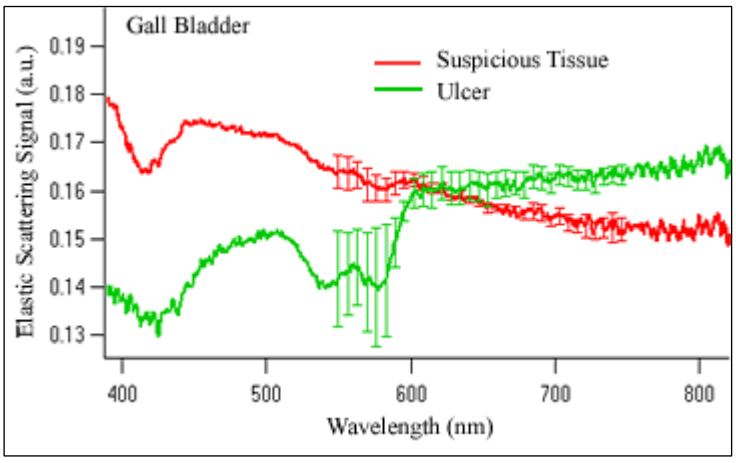

Figure 5.29 ESS spectra of 62 years old male patient's ulcer and chronic colecystit gall bladder

71 years old male patient's gall bladder tissue was diagnosed as acute colecystit. The ESS spectrum of different parts of gall bladder tissue is seen in Figure 5.30. The slopes were calculated between 600 – 750 nm wavelengths because of the blood absorption band in the wavelength range of 550-600 nm. While the slope of ESS spectra of edematous tissue, surface of gall bladder, and muscle tissue are negative (edema: -

62.11 ± 0.54, surface: -151.8 ± 1.59, muscle: -72.63) the slope of ESS spectrum of ulcer is positive (28.32 ± 0.91).

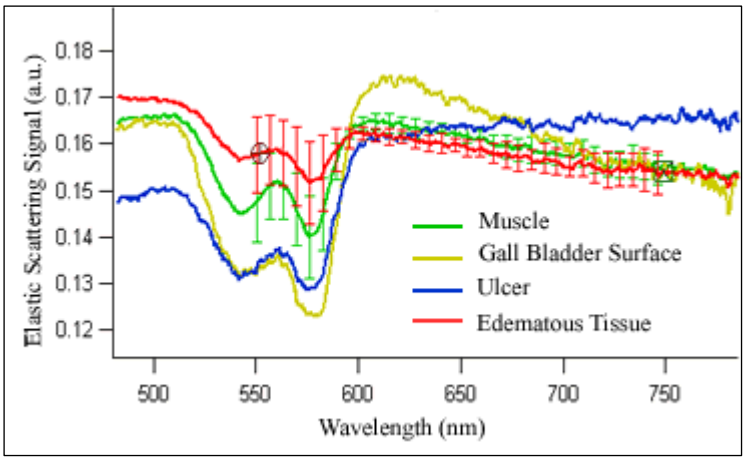

Figure 5.30 ESS spectra of different parts of gall bladder of 71 years old male patient

The stomach of 55 years old female patient was dissected and diagnosed as adeno carsinoma by histopathology. The ESS spectra of tumor, lipid, and normal tissue have negative slopes (tumor: -87.75 ± 0.37, lipid: -86.78 ± 0.53, and normal: -90.45 ± 0.37) (Figure 5.31). The tumor slope is consistent with the expected one. From other measurements it was seen that the ESS spectra of fat had negative slope so this lipid graph is consistent with them. However the ESS spectrum of normal tissue should have positive slope but it has negative.

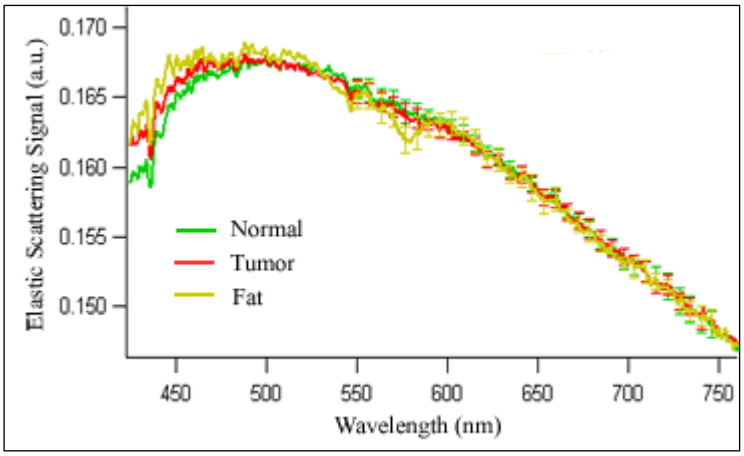

Figure 5.31 ESS spectra of different parts of stomach of 55 years old female patient

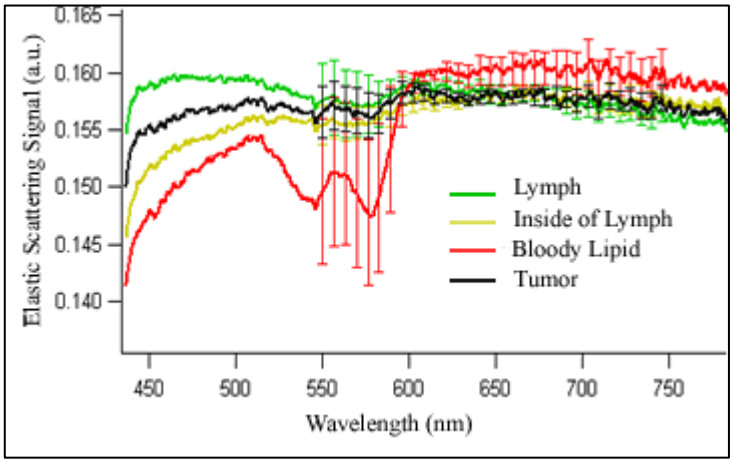

Figure 5.32 ESS spectra of different parts of stomach of 70 years old female patient

The ESS spectra that are taken from different parts of small intestine and mesenter lymph node of 70 years old female patient are seen in Figure 5.32. Lymph node is not cancerous. There is no neoplastic infiltration in tumor, only there are atypical cells according to histopathology report. The slopes were examined in the wavelength range of 600 – 750 nm. The slope of ESS spectrum of lymph is -19.183 ± 0.305, inside of lymph is 60.654 ± 0.4, bloody lipid is -1.9486 ± 0.518, and tumor is -6.5513 ± 0.36 in this wavelength range. The tumor and lipid results are consistent but others are not.

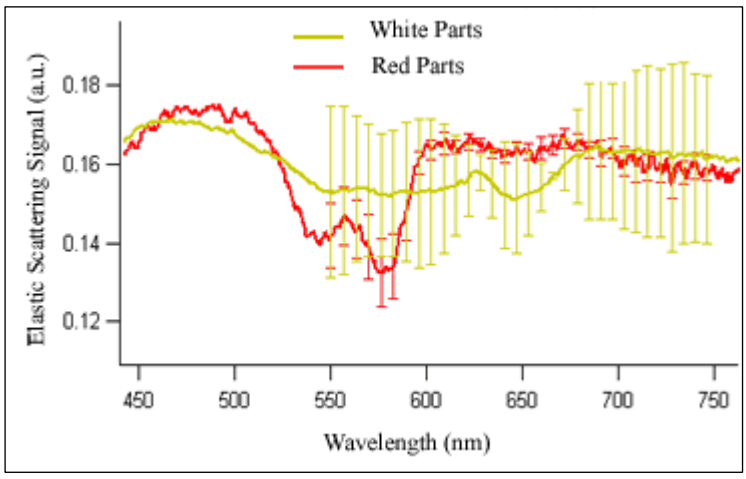

Figure 5.33 ESS spectra of parts of large intestine of 7 years old patient

7 years old patient's large intestine tissue graph is seen in Figure 5.33. The spectra of the large intestine's red parts has negative slope (-46.787 ± 1.98) and white parts have positive slope (86.656 ± 2.92) in the wavelength range of 600 – 750 nm.

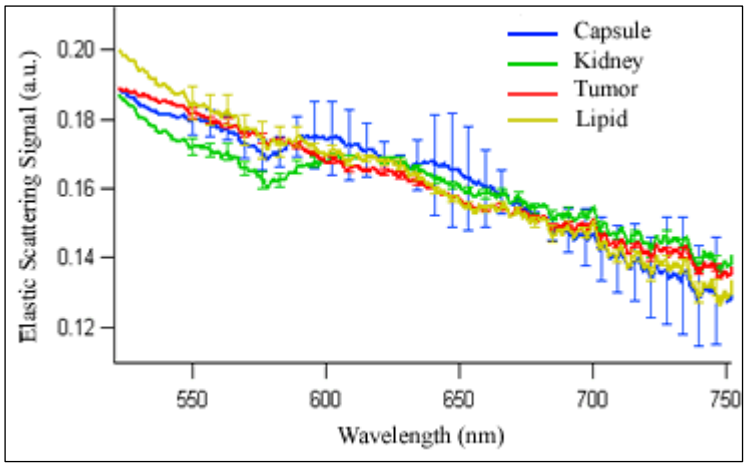

Figure 5.34 ESS spectra of 68 years old male patient's kidney

68 years old male patient's kidney was examined histopathologically and it was diagnosed as carsinoma. The ESS spectrum of different parts of kidney is seen in Figure 5.34. The slope of ESS spectra of capsule, kidney, tumor, and lipid are negative (capsule: -213.3 ± 1.97, kidney: -208.06 ± 1.75, tumor: -229.3 ± 0.44, and lipid: -305.01 ± 1.15) in the visible range. While the graph of tumor and lipid is consistent with the expected one the graph of kidney and capsule is not.

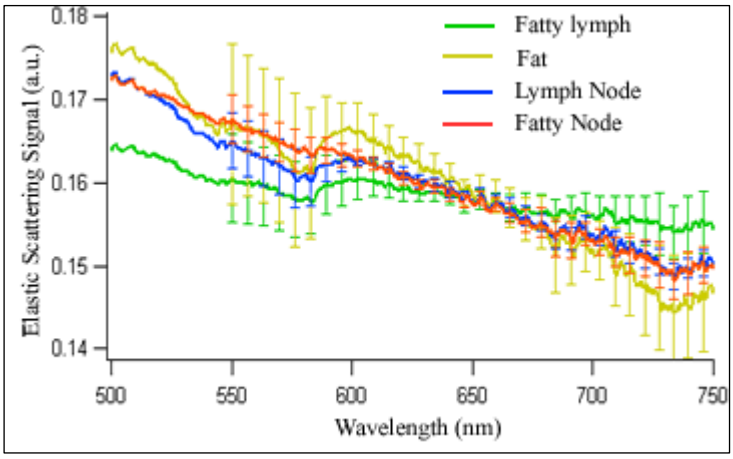

Figure 5.35 ESS spectra of 70 years old male patient's left lymph node of prostate

70 years old male patient's prostate was dissected due to find if there was metastasis in the left lymph node. Tissue was not cancerous according to histopathology. The ESS spectra of different parts of tissue have negative slopes (fatty lymph: -35.16 ± 0.32, fat: -11 ± 0.74, lymph node: -88.9 ± 5.22, and fatty node: -93.44

± 2.26) in the visible range (Figure 5.35). While the graphs of fat and fatty tissues are consistent with the expected one the graph of normal lymph is not.

Ovarian cyst of 50 years old patient was dissected and analyzed. According to the diagnosis of histopathology there were no cancerous lesions. The ESS spectra of both cyst and ovarian tissue have negative slopes (ovarian tissue: -49.272 ± 0.392, cyst: -78.69 ± 0.80) that was expected for cancerous tissue (Figure 5.36).

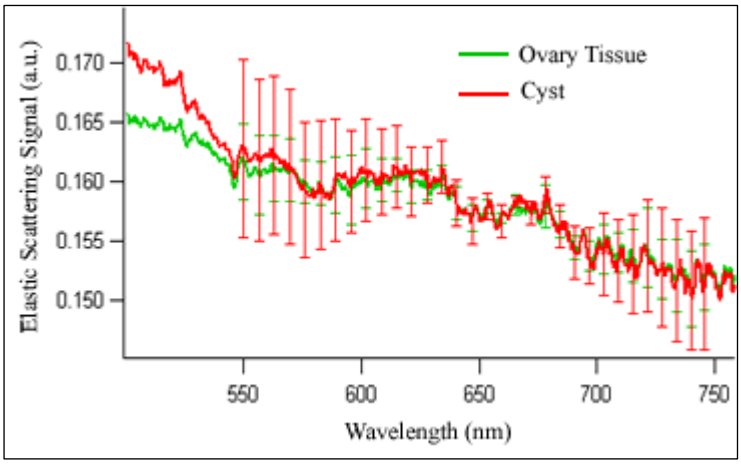

Figure 5.36 ESS spectra of 50 years old female patient's ovarian tissue

48 years old female patient's ovary was examined histopathologically and it was diagnosed as adeno carsinoma. The ESS spectrum of different parts of ovary is seen in Figure 5.37. The slopes of ESS spectra of all parts of cancerous tissue are positive (first part (hard): 101.97 ± 1.26, second part (soft): 171.84 ± 1.21, tumor: third part: 181.67 ± 1.21) in the visible wavelength range. It was expected negative for cancerous tissues.

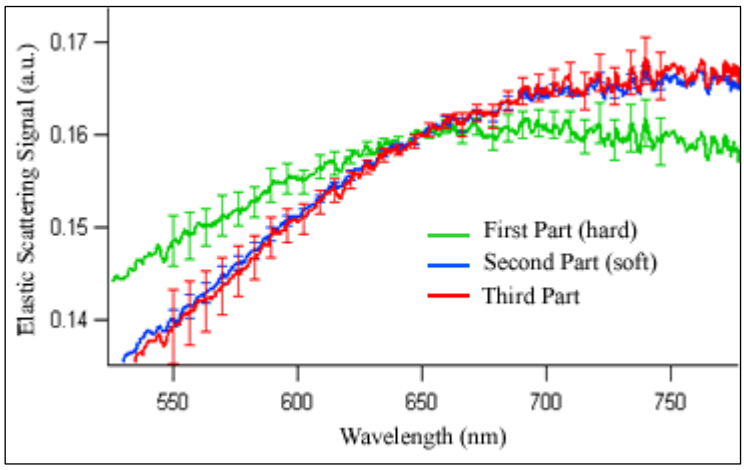

Figure 5.37 ESS spectra of 48 years old female patient's cancerous ovarian tissue

In Figure 5.38 normal spleen tissue of 30 years old male patient is seen. Both spectra have positive slopes (surface: 110.95 ± 5.26, inside: 175.58 ± 5.3) as expected for normal tissues.

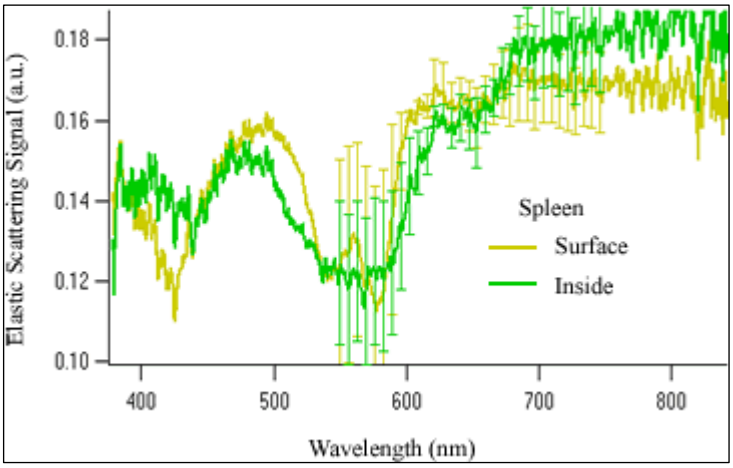

Figure 5.38 ESS spectra of 30 years old male patient' normal spleen

CancerScanner system could not give successful results for these tissues. The predictive value of the system in differentiating tumor and normal for all these tissues was 38.46 % (Table 5.4). The sensitivity and specificity of the CancerScanner system is 78.57 % and 24 % respectively.

Table 5.4

Tissue Type, Number of Patients and Tissues, CancerScanner System Success for some Human Tissues

Tissue Type	Number of Patients	Number of Tissues	Success Diagnosis	Success Rate (%)
Thyroid	5	9	5	55.5
Gall Bladder	2	6	3	33.3
Stomach	1	3	1	33,3
Small Intestine	1	4	2	50
Large Intestine	1	2	1	50
Kidney	1	4	1	25
Prostate	1	4	0	0
Ovary	2	5	0	0
Spleen	1	2	2	100
Total	15	39	15	38.46

5.3. Discussion

Alterations in the structure affect the light scattering properties of the tissue. This study is based on an approach that the morphological alterations of cells such as nuclei enlargement, increased concentration of chromatin, and pleomorphism may be detected by using the spectrum of the light scattered back from the target tissue according to elastic light scattering theory.

It was observed that there were similarities between the experimental results of this study and the Drezek's [35] theoretical model of light scattering in normal and pre-cancerous cervical cells as mentioned in chapter 2 (Figure 2.10). In the simulation, broad band light in the range of 600-1000 nm was used and intensity of scattered light was integrated for different angular ranges as a function of wavelength. The difference between the integrated intensities of normal and pre-cancerous cells is the most dominant for the angular range of 160 – 180 degrees. According to the experimental results of the study on human tissues with CancerScanner system, the intensity of back-scattered light increases with wavelength for normal tissues which is consistent with Drezek's simulation. The intensity of back-scattered light does not change with wavelength for dysplasia in the simulation but decreases for cancerous cells according to results of CancerScanner system.

Table 5.5
Sensitivity and specificity of CancerScanner System

Tissue	Sensitivity (%)	Specificity (%)
Lung & P. Lymph Node	100	66.6
Brain	75	100
Breast	40	30.77
Other Tissues	78.57	24

The results of this study showed that the sensitivity of the CancerScanner system was high for lung and paratracheal lymph nodes (Table 5.5). However the specificity was not high since there were only three normal tissues. More measurements should be taken especially from normal tissues to see if the specificity increases. On the basis of these results a new study on lymph nodes can be suggested. Non-cancerous paratracheal lymph nodes may be saved with this method since these nodes are sacrificed during surgical operation and analyzed pathologically if there is any doubt about lung or thyroid cancer metastasis to the paratracheal lymph nodes.

In brain study CancerScanner system gave expressive results and it was observed that examining elastic scattering signal can be an advantageous method to differentiate brain tumor and normal tissue. Number of measurements on brain tissue should be increased in the future.

One of the important issues for the surgeon is to define the exact place of the tumor and to dissect the whole cancerous lesion. For this purpose surgeons need a diagnosis to see if there are malignant cells in the border of dissected material. During operation pathologist analyzes this material. The results of this study for brain and lung tissue are promising about that since the ESS spectra taken by CancerScanner system has a negative slope when there are malignant cells in the surrounding tissue. This system gives real time results and it is cheap: it uses only a visible light source, a spectrometer, a single optical fiber, and a PC. It can be very advantageous if it is used in operating rooms for real time diagnosis instead of histopathologic examination. Patients may be rescued from waiting for pathologic processes under anesthesia during operation.

The results of experiments on breast tissue were not compatible with the expected graphs. The sensitivity and specificity of the system were very low (Table 5.5). The confounding factor was lipid cells that are larger than other cells. In the breast the fat and normal tissue usually are not separate from each other. Therefore it is not possible to differentiate normal from tumor for fatty tissues such as breast.

There are many other factors affecting scattering light. Beside fat the hemorrhage or mucosa also changed the graph. The experiments on thyroid, ovary, intestine, and stomach did not show adequate results. The success rates on these tissues were not significant. These were preliminary works on cancer detection with CancerScanner system. In future the number of measurements should be increased on different human tissues and different cancer types to obtain a higher success rate.

It is known that by using only a single fiber optical probe, diffuse component of the backscattered light was minimized. In future studies, the advantages of using single optical fiber about specificity may be examined. This probe can easily fit into endoscope channels or biopsy needle so a comparatively small volume is probed allowing for local measurement of particle size. This can reduce the need for dissecting non-cancerous lesions.

6. CONCLUSION

Cancer is one of the most common causes of deaths in this century. Early cancer diagnosis is crucial to diminish the number of deaths; therefore use of optical methods in cancer diagnosis become more important. Optical methods offer non-invasive, cheaper, and real time detection of cancer compared to other diagnostic methods. The CancerScanner system is based on detection of morphological differences between cancerous and normal tissues. Many cancer cells have comparably large nuclei than normal cells; this optical system detects cancer by collecting elastic scattering signal.

In this thesis work firstly the CancerScanner system reliability was tested on lamb brain tissues *in vitro*. When tissue is heated up to a level, the morphology of cells within the tissue changes. The change of optical properties of tissues related to heat deposition causes a difference between ESS spectra of native and coagulated tissue.

In the first study, parts of lamb brains; brainstem, cerebellum, frontal lobe gray matter, and frontal lobe white matter were coagulated at 45 ºC, 60 ºC, and 80 ºC. The ESS spectra that were taken by CancerScanner system of these native and coagulated tissues were analyzed. It was observed that as the coagulation temperature was increased the slope of the ESS spectra decreased from the relatively high positive values of native brain tissues to lower positive values at 45 ºC and 60 ºC, and, even turned to negative at 80 ºC. This showed that the slopes of ESS spectra taken with CancerScanner system in the visible wavelength range give exact information about alterations of tissue optical properties.

When the ESS spectra of native brain tissue parts from three different lamb brains were analyzed it was observed that there is a correlation between the spectra of the same parts of different native brains. Another outcome of this *in vitro* study is that the system can distinguish the four parts of native brain according to the slopes of the ESS spectra. These results verified the reliability of the system and measuring method.

In the second study, system was tested firstly on human tissues *in situ* in order to detect the cancerous lesions. 15 Lungs and paratracheal lymph nodes were examined. The success rate of CancerScanner system in detecting cancerous lesions was 86.6%. The measurements from 10 brain tissues of 7 patients showed that cancer detection success rate of CancerScanner system on brain tissue was 80 %. CancerScanner system could not

distinguish breast tumors from normal tissue since breast was fatty. ESS spectra of both fat and cancerous tissue had negative slopes so the system was not successful on breast tissue. The study on other types of human tissues such as tissues from the thyroid, ovary, intestine, stomach could not give significant results.

The preliminary results of first use of CancerScanner system in clinics were reported in this thesis study. It is concluded that CancerScanner system can be an alternative diagnosis method. However, more measurements must be taken for future use of CancerScanner in medicine.

7. REFERENCES

1. Wilson B. C., Jacques S. L. "Optical Reflectance and Transmittance of Tissues: Principles and Applications" *IEEE Journal of Quantum Electronics*, Vol.26, No.12, pp. 2186-2199, 1990.

2. Sokolov K. et all, "Optical Systems for In Vivo Molecular Imaging of Cancer" *Technology in Cancer Research & Treatment*, Vol. 2, No. 6, pp. 491-504, 2003.

3. Irving J. Bigio and Judith R. Mourant. "Ultraviolet and visible spectroscopies for tissue diagnostics: fluorescence spectroscopy and elastic-scattering spectroscopy" *Phy. Med. Biol.* Vol. 42, pp. 803-814, 1997.

4. Sokolov K., Follen M. Kortum R. R. "Optical Spectroscopy for detection of neoplasia" *Current Opinion in Chemical Biology*, Vol. 6, pp. 651-658, 2002.

5. Rajan S. Gurjar, Vadim Backman, Lev T. Perelman, Iren Georgakoudi, Kamran Badizadegan, Irving Itzkan, Ramachandra R. Dasari, Michael S. Feld. "Imaging Human Epithelial Properties with Polarized Light Scattering Spectroscopy" *Nature Medicine*, Vol. 7, No. 11. pp. 1245-1248, 2001.

6. Backman V. et all, "Measuring Cellular Structure at Submicrometer Scale with Light Scattering Spectroscopy" *IEEE Journal on Selected Topics in Quantum Electronics*, Vol. 7, No. 6, pp. 887-893, 2001.

7. Perelman L. T. et all. "Observation of Periodic Fine Structure in Reflectance from Biological Tissue: A New Technique for Measuring Nuclear Size Distribution" *Physical Review Letters***,** Vol. 80, No. 3. pp. 627-630, 1998.

8. Wax A., Yang C., Backman V., Badizadegan K., Boone C. W., Dasari R. R., Feld M. S., "Cellular Organization and Substructure Measured Using Angle-Resolved Low-Coherence Interferometry" *Biophysical Journal*, Vol. 82, pp. 2256-2264, 2002.

9. Pyhtila J. W., Graf R. N., Wax A. "Determining nuclear morphology using an improved angle-resolved low coherence interferometry system" Optics Express, Vol. 11, No. 25, pp. 3473 – 3484, 2003.

10. Craig F. Bohren, Donald R. Huffman, *Absorption and Scattering of Light by Small Particles*, A Willey Interscience Publication, 1998.

11. H. C. van de Hulst, *Light Scattering by Small Particles*, New york, Wiley, 1981.

12. Max Born, Emil Wolf, *Principles of Optics*, 7th Edition, Cambridge Univ. Press. 1999.

13. Canpolat M., Mourant J. R. "Particle Size Analysis of Turbid Media with Single Optical Fiber in Contact with the Medium to Deliver and Detect White Light" *Applied Optics*, Vol. 40, No. 22, pp. 3792-3799, 2001.

14. Dunn A., Richards-Kortum R., "Three-Dimensional Computation of Light Scattering From Cells" *IEEE Journal of Selected Topics in Quantum Electronics*, Vol.2, No. 4, 1996.

15. *United States Patent Application Publication*, Canpolat et al., Pub. No: US 2002/0165456 A1, Pub. Date: Nov.7, 2002.

16. Graham Currie, Angela Curie, *Cancer the biology of malignant disease*, Edward Arnold (Publishers) Ltd. London, 1982.

17. Richard E. LaFond, Editor, *Cancer: the Outlaw Cell*, American Chemical Society, Washington, DC. Second Edition. (1988)

18. *Turkish Association for Cancer Research and Control*, http://www.turkcancer.org

19. *University of Florida PA Program*, Introduction to Medicine. http://medinfo.ufl.edu/pa/chuck/fall/handouts/injury.htm

20. Roger J.B. King, *Cancer Biology*, Addison Wesley Longman Limited, England, 1996.

21. Leslie Roberts, *Cancer Today Origins, Prevention, and Treatment*, Institute of Medicine/National Academy Press, Washington, D.C., 1984.

22. H.Zeng, A. McWilliams, S. Lam. "Optical Spectroscopy and imaging for early lung cancer detection: a review" *Photodiagnosis and Photodynamic Therapy*, Vol. 1, pp. 111-122, 2004.

23. M. Panjehpour, C. E. Julius, M. N. Phan, T. Vo-Dinh, S. Overholt, "Laser-Induced Fluorescence Spectroscopy for In Vivo Diagnosis of Non-melanoma Skin Cancers" *Lasers in Surgery and Medicine* Vol. 31, pp. 367–373, 2002.

24. Hung J, Lam S, LeRiche JC, et al. "Autofluorescence of normal and malignant bronchial tissue" *Lasers Surg Med*. Vol. 11, pp. 99–105, 1991.

25. Cothren RM, Richards-Kortum R, Sivak MV, et al. "Gastrointestinal tissue diagnosis by laser-induced fluorescence spectroscopy at endoscopy" *Gastrointest Endosc.* Vol. 36, pp. 105–111, 1990.

26. C.S. Betz, M. Mehlmann, K. Rick, H. Stepp, G. Grevers, R. Baumgartner, A. Leunig **"**Autofluorescence imaging and spectroscopy of normal and malignant mucosa in patients with head and neck cancer" *Lasers in Surgery and Medicine* Vol. 25, No. 4, pp. 323-334, 1999.

27. D.C.G. De Veld, M.J.H. Witjes, H.J.C.M. Sterenborg, J.L.N. Roodenburg. "The status of in vivo autofluorescence spectroscopy and imaging for oral oncology" Vol. 41, pp. 117-131, 2005.

28. J. Y. Qu, P. Wing, Z. Huang, D. Kwong, J. Sham, S. L. Lee, W. K. Ho, W. I. Wei "Preliminary study of in vivo autofluorescence of nasopharyngeal carcinoma and normal tissue" *Lasers in Surgery and Medicine*, Vol. 26, No. 5, pp. 432-440, 2000.

29. Valery Tuchin, *Tissue Optics Light Scattering Methods and Instruments for Medical Diagnosis*, SPIE Tutorial Texts in Optical Engineering, Vol. TT38, SPIE Press, Bellingham, 2000.

30. Adam Liebert, Roman Maniewski, *Scattering*, Polish Academy of Science, Warsaw, Poland. Encyclopedia of Optical Engineering, 2003.

31. Valery V. Tuchin, *Biomedical Spectroscopy*, Encyclopedia of Optical Engineering DOI: 10.1081/E-EOE 120009763, 2003.

32. Z. Chen, A. Taflove, V. Backman, "Equivalent volume-averaged light scattering behavior of randomly inhomogeneous dielectric spheres in the resonant range" *Optics Letters*, Vol.28, No.10, 2003.

33. A. H. Hielscher, J. R. Mourant, I.J. Bigio. "Biomedical Diagnostics with Elastic Light Scattering in Cell Suspensions and Tissues" *Proceedings-19th International Conference, IEEE/EMBS*, 1997.

34. Judith R. Mourant, Andreas H. Hielscher, Angelia A. Eick, Tamara M. Johnson, James P. Freyer, "Evidence of Intrinsic Differences in the Light Scattering Properties of Tumorigenic and Nontumorigenic Cells" *Cancer (Cancer Cytopathology)* Vol. 84, No. 6, 1998.

35. R.Drezek, A. Dunn, R. R. Kortum, "A Pulsed Finite-Difference Time-Domain (FDTD) Method for Calculating Light Scattering from Biological Cells Over Broad Wavelength Ranges" *Optics Express*, Vol. 6, No.7, 2000.

36. V. Backman, R. Gurjar, K. Badizadegan, I. Itzkan, R. R. Dasari, L. T. Perelman, M. S. Feld. "Polarized Light Scattering Spectroscopy for Quantitative Measurement of Epithelial Cellular Structures *in Situ*" *IEEE Journal of Selected Topucs in Quantum Electronics*, Vol. 5, No. 4, 1999.

37. Y. L. Kim, Y. Liu, R. K. Wali, H. K. Roy, M. J. Goldberg, A. K. Kromine, K. Chen, V. Backman, "Light Scattering Fingerprints of Initial Pre-dysplastic Events in Colon Carcinogenesis" *Proceedings of the 25th Annual International Conference of the IEEE EMBS*, Vol.17, No.21, 2003.

38. T. Papaioannou, N. Preyer, Q. Fang, H. Kurt, M. Carnohan, R. Ross, A. Brightwell, G. Cottone, L. Jones, L. Marcu, " Performance evaluation of fiber optic probes for tissue lifetime fluorescence spectroscopy"*Advanced Biomedical and Clinical Diagnostic Systems*, Proceedings of SPIE Vol. 4958, 2003.

39. T. J. Pfefer, K. T. Schomacker, M. N. Ediger, N. S. Nishioka, “Light Propagation in Tissue During Fluorescence Spectroscopy With Single-Fiber Probes” *IEEE Journal on Selected Topics in Quantum Electronics*, Vol. 7, No. 6, 2001.

40. P. R. Bargo, S. A. Prahl, S. L. Jacques, “Collection Efficiency of a Single Optical Fiber in Turbid Media” *Applied Optics*, Vol. 42, No. 16, 2003.

41. A. Amelink, M. P. L. Bard, S. A. Burgers, H. J. C. M. Sterenborg, “Single-scattering Spectroscopy for the Endoscopic analysis of particle size in Superficial Layers of Turbid Media” *Applied Optics*, Vol. 42, No. 19, 2003.

42. T. P. Moffitt and S. A. Prahl, “Sized-fiber reflectometry for measuring local optical properties,” *IEEE J. Quantum Electron*. Vol. 7, pp. 952–958, 2001.

43. A N Yaroslavsky, P C Schulze, I V Yaroslavsky, R Schober, F Ulrich, H-J Schwarzmaier, “Optical properties of selected native and coagulated human brain tissues *in vitro* in the visible and near infrared spectral range” *Phys. Med. Biol*. Vol. 47 pp. 2059–2073, 2002.